JOURNAL OF PETROLOGY | VOLUME 44 | NUMBER 1 | PAGES 159–195 | 2003

Magma Genesis and Mantle Heterogeneity in the Manus Back-Arc Basin, Papua New Guinea

JOHN M. SINTON[1]*, LORI L. FORD[1]†, BRUCE CHAPPELL[2] AND MALCOLM T. McCULLOCH[3]

[1]DEPARTMENT OF GEOLOGY AND GEOPHYSICS, UNIVERSITY OF HAWAII, 1680 EAST–WEST ROAD, HONOLULU, HI 96822, USA

[2]DEPARTMENT OF GEOLOGY, AUSTRALIAN NATIONAL UNIVERSITY, CANBERRA, A.C.T. 0200, AUSTRALIA

[3]RESEARCH SCHOOL OF EARTH SCIENCE, AUSTRALIAN NATIONAL UNIVERSITY, CANBERRA, A.C.T. 0200, AUSTRALIA

RECEIVED MAY 29, 2001; REVISED TYPESCRIPT ACCEPTED JULY 23, 2002

Geochemical data from back-arc volcanic zones in the Manus Basin are used to define five magma types. Closest to the New Britain arc are medium-K lavas of the island arc association and back-arc basin basalts (BABB). Mid-ocean ridge basalts (MORB), BABB and mildly enriched T-MORB (transitional MORB) occur along the Manus Spreading Center (MSC) and Extensional Transform Zone (ETZ). The MSC also erupted extreme back-arc basin basalts (XBABB), enriched in light rare earth elements, P, and Zr. Compared with normal MORB, Manus MORB are even more depleted in high field strength elements and slightly enriched in fluid-mobile elements, indicating slight, prior enrichment of their source with subduction-related components. Chemical variations and modeling suggest systematic, coupled relationships between extent of mantle melting, prior depletion of the mantle source, and enrichment in subduction-related components. Closest to the arc, the greatest addition of subduction-related components has occurred in the mantle with the greatest amount of prior depletion, which has melted the most. Variations in K_2O/H_2O indicate that the subduction-related component is best described as a phlogopite and/or K-amphibole-bearing hybridized peridotite. Magmas from the East Manus Rifts are enriched in Na and Zr with radiogenic $^{87}Sr/^{86}Sr$, possibly indicating crustal interaction in a zone of incipient rifting. The source for XBABB and lavas from the Witu Islands requires a mantle component similar to carbonatite melt.

KEY WORDS: *Manus back-arc basin, mantle metasomatism, magma generation*

INTRODUCTION

It has long been known that the diversity of rock types and chemical lineages in extensional back-arc basins greatly exceeds that of mid-ocean ridges. Although lavas generally similar to mid-ocean ridge basalts (MORB) are known from several back-arc basins, a broad range of other rock types also have been found. Several workers have emphasized enrichments in certain volatile and lithophile elements compared with MORB (e.g. Tarney *et al.*, 1977; Garcia *et al.*, 1979; Fryer *et al.*, 1981; Sinton & Fryer, 1987). Fryer *et al.* (1981) argued that the chemical signature of lavas erupted in back-arcs is unique to that setting and proposed the term back-arc basin basalts (BABB) to denote this magma series. However, the exact nature and cause of the mantle source enrichment has led to various competing models for the petrogenesis of lavas in back-arc basins. Most of these models involve source component mixing, with one component generally accepted to be depleted asthenosphere similar to, or even more depleted than, the source for typical MORB. The nature of the other components varies with author and/or basin. Several workers have argued that BABB have concentrations of incompatible and volatile elements that are intermediate between MORB and those in island arcs lavas, and hence, have called on the subducted slab for the source of a component contributing to the composition of BABB. Sinton & Fryer (1987) emphasized

*Corresponding author. Telephone: 808-956-7751. Fax: 808-956-5512. E-mail: sinton@hawaii.edu
†Present address: 173 Kuuala Street, Kailua, HI 96822, USA.

some differences between BABB and arc lavas and proposed that the component giving rise to BABB in the Mariana Trough was derived from dehydration of the deepest part (>300 km) of the subducted slab.

Although some systematic relationships can be found in island arcs between lava composition and depth to the subducted slab (e.g. Tatsumi, 1989; Plank & Langmuir, 1992), spatial relationships within back-arc basins appear to be less direct (e.g. Saunders & Tarney, 1979; Taylor & Karner, 1983; Johnson & Sinton, 1990; Price *et al.*, 1990). In the East Scotia Sea, lavas with BABB compositions have been erupted along a spreading center that is displaced several hundred kilometers laterally from the deepest part of the subducted slab. There is evidence that the longest-lived and best-organized spreading centers in the central Lau Basin, North Fiji Basin and Manus Basin dominantly erupt MORB lavas with little or no BABB signature. This relationship suggests that the BABB source component has a low melting temperature that can be 'melted out' by prolonged spreading center processes remote from subducted lithosphere.

Representative lava collections from back-arc basins have now been obtained for a large number of locations. The diversity of lava types acquired indicates that a wide range of magma source compositions and melt generating processes are possible in back-arc settings. However, BABB magmas are present in all these locations and share a common set of geochemical characteristics. These include moderate enrichments (relative to MORB) in H_2O, alkalis and other large ion lithophile elements, slight depletions in Ti, Nb and Y, and essentially flat rare earth element (REE) patterns at total abundances varying from ~5 to 20 times chondrite values. This last characteristic is interesting because it occurs in all back-arc basins, despite widely varying REE patterns in associated island arcs.

In this paper we present new major and trace element and isotopic data on lavas from the Manus Basin, a back-arc basin behind the New Britain island arc in Papua New Guinea (Fig. 1). There is a well-documented variation in the chemistry of the subaerial New Britain island arc (e.g. Johnson, 1977; Johnson & Arculus, 1978; Woodhead & Johnson, 1993; Woodhead *et al.*, 1998), which makes the combined New Britain arc–Manus back-arc system of particular interest. Within the Manus Basin, a wide range of lava types have been erupted that are systematically disposed to tectonic elements in the back-arc extensional zones (Fig. 2).

We use both petrological and geochemical data to assess the nature of the source components and melting processes required to produce the back-arc magma types. These results are then combined with data from the New Britain arc to produce a more comprehensive view of magmatic processes occurring in this arc–back-arc system.

SAMPLING AND ANALYTICAL METHODS

Samples for this study were obtained from 34 rock dredges and two bottom camera runs during R.V. *Moana Wave* Cruise MW8518, and from samples collected by the *Mir* submersible and coring operations of the 23rd Cruise of the R.V. *Akademik Mstislav Keldysh* (Crook *et al.*, 1997). Sample locations and recoveries are given in Table 1 and shown in Fig. 2. All sample sites were located on targets with highly reflective side-scan sonar backscatter, indicating relatively young age. The Manus Basin is a region of very high, but generally unknown sedimentation rate. However, it is apparent that the highest reflectivity is restricted to regions within about 5–6 km of the Manus Spreading Center (MSC) ridge axis, where full spreading rates range up to 92 mm/yr (Martinez & Taylor, 1996). This suggests that the seafloor with highest reflectivity is less than ~130 kyr old. Most recovered samples are essentially devoid of Mn encrustations, an observation that generally supports the interpretation that the samples recovered in this program are all very young. Thus, geochemical interpretations based on these data can be considered to pertain to more or less coeval processes occurring in the Manus Basin within the last 130 kyr.

Glass analyses

Nearly all the studied samples have fresh glassy selvages. Because unaltered glasses are unambiguously quenched liquids, glass analytical data can be used to define chemical types and liquid lines of descent without considering phenocryst accumulation or alteration processes. We have analyzed 206 glassy samples for major and minor elements with the automated, wavelength-dispersive, three-spectrometer Cameca MBX microprobe at the University of Hawaii. Oxides were calibrated against natural glass standards VG-2 (Makaopuhi lava lake) and A-99 (Juan de Fuca Ridge); MnO and P_2O_5 were calibrated against rhodonite and apatite, respectively. All analyses used a defocused beam (~25 μm), 15 kV accelerating voltage and a sample current of 12 nA. Count times were 50 s for P_2O_5 and 10 s for all other elements. A minimum of six spot analyses, typically on several glass chips, were determined for each sample, and the resulting values averaged and normalized to the glass standards. Samples from single dredges that gave identical results within analytical precision were combined into groups, assuming that they represent samples from the same lava flow or closely related flows. A total of 66 groups are defined by the glass data; arithmetic means for each group are presented in Table 2, along with estimated precision of the data based on variance from the mean for the well-analyzed Group 16.

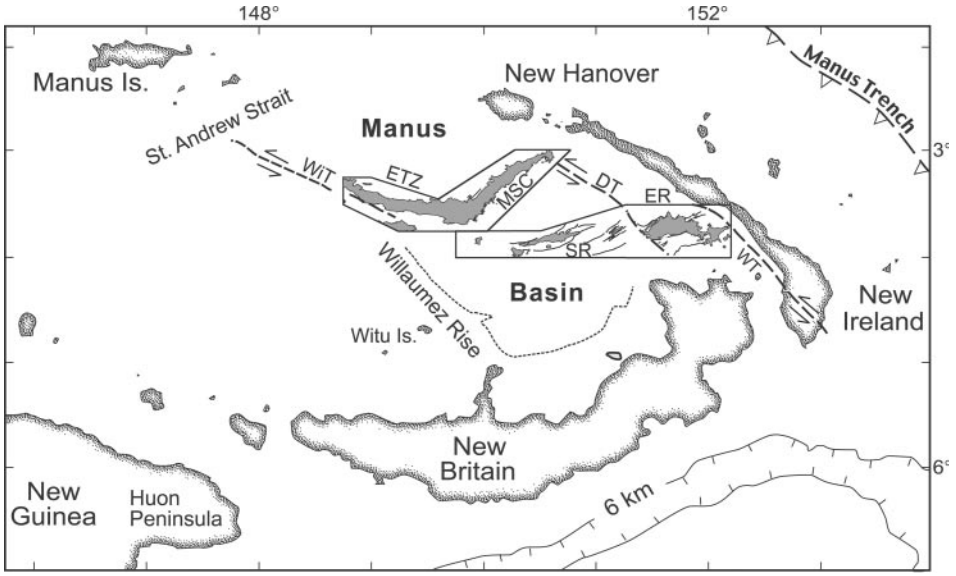

Fig. 1. Regional map of the Manus Basin–New Britain area. Active volcanism occurs within the back-arc basin along the East Manus Rifts (ER), Southern Rifts (SR), Manus Spreading Center (MSC) and Extensional Transform Zone (ETZ) (after Martinez & Taylor, 1996). WiT, DT and WT refer to the Willaumez, Djaul and Weitin Transforms, respectively. The areas shown in Fig. 2 are outlined. The currently inactive Manus Trench is the former site of southward subduction, which ceased at ~10 Ma. Current subduction is occurring along the deep trench (>6 km) located to the south of New Britain.

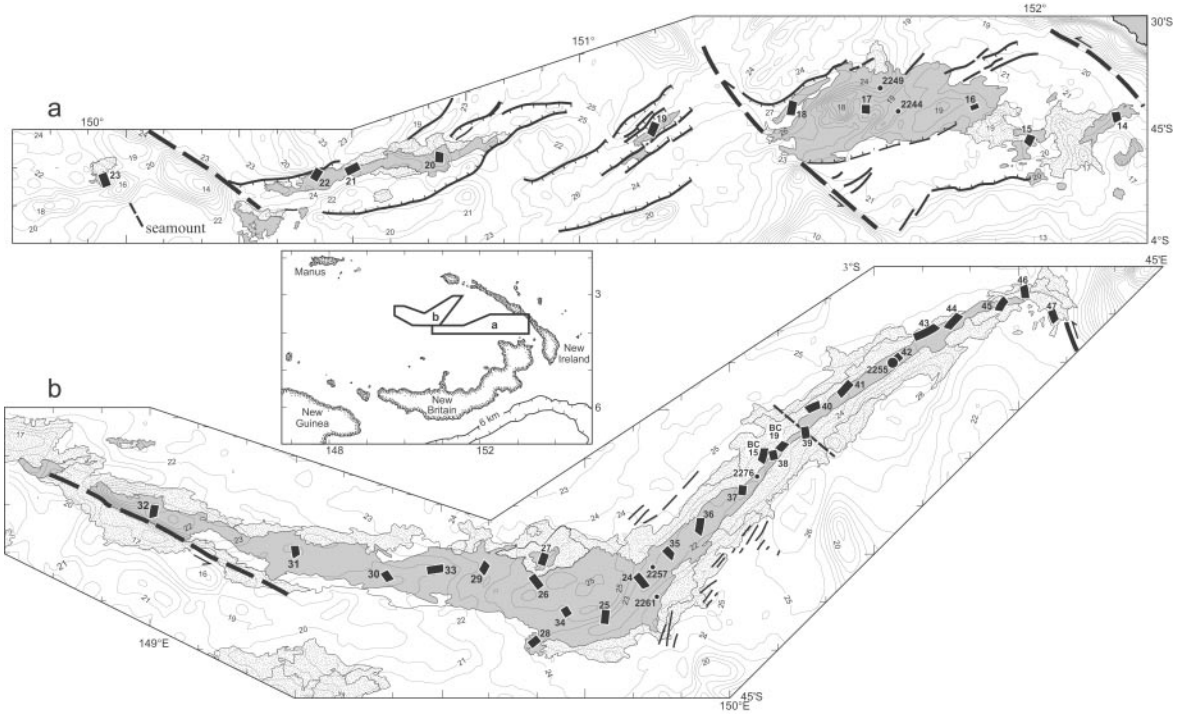

Fig. 2. Active zones in the Manus Basin showing all sample locations discussed in the text. Heavy bars are dredges from cruise MW8516; circles denote gravity cores from *Keldysh* Cruise 21. Shaded areas denote regions of high side-scan sonar reflectivity; stippled areas show slightly lower reflectivity. These zones represent the areas of youngest seafloor. The MSC can be divided into two chemically distinct segments with boundary denoted by the dashed line near dredge 39. (See text for discussion.)

Table 1: Sample station summary

Station	Latitude	Longitude	Depth (m)	Recovery
RD 14	3°42·9′S	152°10·4′E	1755–1950	40 kg vesicular, aphyric, glassy basaltic andesite and andesite; 2 pieces pumice; 3 pieces hyaloclastic breccia
RD 15	3°46·7′S	151°59·0′E	1700–2025	40 kg phyric vesicular basalt; 5 kg pumice
RD 16	3°42·1′S	151°52·4′E	1980–2065	55 kg glassy vesicular basaltic andesite
RD 17	3°44·4′S	151°38·8′E	1685–1860	40 kg aphyric, vesicular andesite and dacite
RD 18	3°42·3′S	151°27·8′E	2580–2730	35 kg vesicular, plag-phyric pillow basalt; 3 pieces pumice
RD 19	3°45·1′S	151°09·5′E	2625–2635	35 kg vesicular, phyric basalt; 6 pieces mudstone
RD 20	3°48·8′S	150°41·6′E	2045–2080	30 kg glassy oliv + plag-phyric pillow basalt
RD 21	3°50·4′S	150°30·1′E	2400–2465	30 kg vesicular, phyric basalt; 1 piece pumice
RD 22	3°51·5′S	150°25·8′E	2530–2580	15 kg basaltic lava including highly vesicular, weakly plag-phyric and sparsely vesicular, ol-phyric types
RD 23	3°52·4′S	149°58·0′E	1390–1865	12 kg ol-phyric pillow basalt
RD 24	3°32·7′S	149°51·4′E	2155–2185	50 kg glassy lavas incl. non-vesicular ol + plag-phyric ferrobasalt and vesicular plag-phyric andesite
RD 25	3°36·5′S	149°47·8′E	2215–2255	55 kg aphyric pillow basalt and ferrobasalt
RD 26	3°32·8′S	149°40·7′E	2475–2570	50 kg aphyric pillow basalt
RD 27	3°30·3′S	149°41·7′E	2520–2535	1 kg very glassy pillow basalt
RD 28	3°39·4′S	149°40·4′E	2370–2440	1·5 kg glassy pillow basalt and basaltic andesite glass fragments
RD 29	3°31·4′S	149°34·2′E	2220–2415	50 kg glassy phyric pillow basalt
RD 30	3°32·3′S	149°24·5′E	1885–1975	80 kg vesicular basalt to andesite
RD 31	3°30·1′S	149°15·5′E	2075–2245	110 kg ferrobasalt pillows
RD 32	3°25·2′S	149°00·9′E	2300–2420	100 kg phyric pillow basalt
RD 33	3°31·7′S	149°28·7′E	2090–2115	25 kg vesicular and non-vesicular ferrobasalt
RD 34	3°36·4′S	149°43·9′E	2445–2510	1 kg pillow basalt
RD 35	3°30·2′S	149°53·8′E	2090–2125	60 kg highly vesicular basaltic andesite and andesite
RD 36	3°26·8′S	149°57·8′E	2155–2165	65 kg phyric basalt and aphyric vesicular andesite
RD 37	3°22·7′S	150°01·6′E	2175–2185	50 kg glassy ferrobasalt pillows
RD 38	3°19·9′S	150°04·9′E	2200–2225	70 kg glassy ferrobasalt sheet lavas and ‘older’ pillows
RD 39	3°17·4′S	150°07·7′E	2285–2370	50 kg glassy ferrobasalt pillows
RD 40	3°14·9′S	150°07·7′E	2300–2310	2 kg glassy basalt sheet lava
RD 41	3°12·0′S	150°12·5′E	2375–2400	45 kg vesicular phyric pillow basalt and aphyric, massive dacite glass
RD 42	3°09·6′S	150°17·1′E	2480–2490	2 kg glassy ferrobasalt
RD 43	3°08·0′S	150°19·3′E	2510–2545	2 kg glassy ferrobasalt
RD 44	3°05·2′S	150°23·7′E	2600–2630	5 kg phyric ferrobasalt pillows; 3 pieces pumice
Rd 45	3°03·9′S	150°27·3′E	2570–2670	20 kg phyric, vesicular dacite and nonvesicular ferrobasalt
RD 46	3°02·0′S	150°30·4′E	2510–2560	50 kg ferrobasalt pillows and sheets; mudstones
RD 47	3°04·6′S	150°33·8′E	2525–2580	1 kg glassy ferrobasalt and pumice
BC 15	3°18·8′S	150°05·8′E	2225–2265	2 glassy ferrobasalts
BC 19	3°06·8′S	150°21·5′E	2580–2600	1 phyric ferrobasalt pillow
2244	3°42·5′S	151°41·7′E	1926	glass chips
2249	3°39·5′S	151°39·4′E	2266	glass chips
2255	3°09·8′S	150°16·8′E	2500	basalt from *Mir* dive
2257	3°31·4′S	149°52·5′E	2131	glass chips
2261	3°34·5′S	149°53·0′E	2468	glass chips
2266	3°06·6′S	150°21·6′E	2628	basalt from *Mir* dive
2276	3°22·2′S	150°02·5′E	2200	7 basalt pieces from *Mir* dive

RD samples from *Moana Wave* Cruise 8518; all others from *Akademik Mstislav Keldysh*, Cruise 21.

Table 2: Glass compositional data

Group	*n*	Setting	Type	SiO_2	TiO_2	Al_2O_3	FeO*	MnO	MgO	CaO	Na_2O	K_2O	P_2O_5	H_2O	S	Cl	F	Total
14A	2	ER	A1	53·3	0·67	15·6	10·2	0·14	4·90	9·30	2·86	0·43	0·14	1·175	0·002	0·171	0·007	98·9
14B	4	ER	A1	62·3	0·83	14·5	7·23	0·15	1·79	5·06	4·12	1·02	0·24	1·813	0·000	0·289	0·008	99·4
15	10	ER	A2	53·3	0·46	15·3	9·98	0·18	5·03	9·66	2·07	1·34	0·25					97·6
16	11	ER	A2	54·8	0·59	15·8	7·80	0·14	5·50	9·80	2·73	0·78	0·16	1·617	0·004	0·297	0·007	100·0
17A	4	ER	A2	63·5	0·89	14·8	5·97	0·15	1·68	4·53	4·50	1·37	0·23	1·590	0·005	0·350	0·007	99·5
17B	2	ER	A2	67·6	0·77	13·5	4·91	0·13	0·82	3·23	4·65	1·69	0·12	1·504	0·000	0·303	0·006	99·2
2244		ER	A2	59·5	1·00	15·4	8·32	0·17	2·48	6·12	3·73	1·02	0·45					98·10
18A	1	ER	Be	51·6	0·49	16·7	8·06	0·08	6·54	12·5	1·83	0·31	0·14					98·3
18B	5	ER	Be	53·9	0·63	15·5	8·99	0·13	5·70	10·7	2·30	0·35	0·18					98·3
2249		ER	Be	52·0	0·43	15·9	7·97	0·16	7·10	12·5	1·78	0·25	0·08					98·2
19	8	SR	Bs	53·6	1·01	14·6	10·6	0·18	4·80	9·49	2·65	0·21	0·16	1·502	0·034	0·059	0·003	98·9
20	3	SR	Bs	51·8	0·68	15·8	8·11	0·14	7·33	12·7	2·00	0·23	0·16					99·0
21	2	SR	Bs	51·6	0·71	15·0	10·0	0·17	6·39	11·5	2·18	0·32	0·13	1·196	0·069	0·147	0·012	99·5
22A	3	SR	Bs	50·6	0·53	16·9	7·67	0·14	7·80	12·7	1·87	0·22	0·14	1·502	0·027	0·117	0·006	100·2
22B	7	SR	Bs	51·4	1·12	14·9	9·93	0·15	6·87	11·6	2·31	0·12	0·15					98·5
23	4	Smt	Ms	48·6	0·68	17·3	9·69	0·18	8·84	13·0	2·10	0·02	0·12	0·072	0·066	0·023	0·002	100·7
24A	4	MSC	M1	51·3	1·39	13·9	12·6	0·19	6·77	11·6	2·36	0·06	0·11					100·1
24B	6	MSC	X3	58·0	1·00	15·0	7·90	0·12	3·63	7·40	3·69	0·56	0·18	1·828	0·000	0·190	0·012	99·5
25A	1	MSC	M1	50·1	1·03	14·9	9·91	0·15	7·94	12·6	2·12	0·03	0·15					98·9
25B	3	MSC	M1	51·1	1·47	13·5	13·0	0·21	6·43	10·8	2·43	0·06	0·15					99·1
26	6	ETZ	M1	51·1	1·04	14·2	10·9	0·20	7·38	12·2	2·10	0·05	0·16					99·3
27	3	ETZ	M1	50·5	1·16	14·1	11·3	0·20	7·30	12·0	2·11	0·04	0·16					98·8
28A	2	MSC	B	51·0	1·12	14·7	11·1	0·17	6·80	11·7	2·20	0·12	0·18					99·1
28B	1	MSC	B	55·5	0·96	16·4	7·81	0·14	4·42	9·09	3·22	0·17	0·17					97·9
29A	1	ETZ	M1	50·8	1·02	15·0	10·6	0·21	8·16	12·7	2·17	0·04	0·15	0·187	0·068	0·046	0·005	101·1
29B	4	ETZ	B	52·0	0·77	16·0	7·82	0·13	6·87	12·0	2·27	0·13	0·13					98·1
30A	3	ETZ	B	53·0	1·12	14·9	10·8	0·20	5·17	9·45	2·95	0·17	0·16					97·8
30B	2	ETZ	B	52·7	1·40	14·0	12·9	0·19	4·45	8·77	3·05	0·16	0·15					97·7
30C	1	ETZ	B	54·1	1·50	13·6	13·0	0·23	3·89	8·04	3·25	0·22	0·17					98·0
31A	2	ETZ	E	50·0	1·64	14·0	11·9	0·23	6·67	11·5	2·67	0·12	0·19	0·614	0·091	0·067	0·008	99·5
31B	4	ETZ	M1	50·9	1·33	14·1	12·4	0·19	7·20	11·6	2·38	0·05	0·16					100·2
31C	1	ETZ	B	50·3	0·40	15·7	7·07	0·09	8·25	13·7	1·48	0·08	0·13	1·152	0·022	0·049	0·003	98·4
32	5	ETZ	M1	50·3	1·04	14·7	10·6	0·16	7·89	12·5	2·23	0·05	0·16					99·6
33A	3	ETZ	M1	51·4	1·09	14·2	11·4	0·18	7·35	12·6	2·30	0·02	0·15					100·7

Table 2: continued

Group	*n*	Setting	Type	SiO_2	TiO_2	Al_2O_3	FeO*	MnO	MgO	CaO	Na_2O	K_2O	P_2O_5	H_2O	S	Cl	F	Total
33B	2	ETZ	B	53·3	1·38	14·8	12·5	0·20	4·15	8·86	3·20	0·22	0·20	1·243	0·023	0·130	0·003	100·1
34	1	ETZ	B	51·2	0·94	14·7	10·6	0·16	7·19	12·3	2·14	0·07	0·13					99·4
35A	6	MSC	X1	55·8	0·83	16·1	7·16	0·12	4·73	9·14	3·27	0·68	0·28	1·578	0·011	0·124	0·007	99·8
35B	2	MSC	X3	58·0	1·05	14·5	8·56	0·11	4·30	7·79	3·53	0·63	0·17					98·6
35C	1	MSC	Xc	61·6	0·90	15·5	5·96	0·12	2·10	5·13	4·51	1·29	0·40					97·5
36A	2	MSC	M1	51·0	1·00	14·9	10·1	0·17	8·45	12·6	2·15	0·05	0·16	0·303	0·064	0·084	0·005	101·1
36B	1	MSC	M1	50·7	1·29	13·8	12·2	0·19	6·79	11·6	2·14	0·05	0·16					98·9
36C	4	MSC	M1	51·7	2·03	13·4	14·1	0·18	5·52	9·98	2·86	0·10	0·22	0·601	0·114	0·146	0·014	100·9
36D	3	MSC	X2	56·1	0·88	16·1	7·45	0·13	5·05	8·79	3·34	0·64	0·24	1·704	0·007	0·155	0·012	100·6
37	9	MSC	M1	50·8	1·21	14·1	11·7	0·17	7·37	11·4	2·26	0·05	0·17					99·2
38A	3	MSC	M1	51·5	1·50	12·8	13·6	0·23	6·66	11·3	2·46	0·04	0·17					100·3
38B	2	MSC	B	52·5	1·19	14·5	12·0	0·18	5·84	10·2	2·60	0·18	0·20					99·4
38C	2	MSC	B	52·6	1·40	13·2	13·2	0·20	5·52	9·89	2·74	0·19	0·18	1·243	0·074	0·148	0·005	100·6
39A	3	MSC	M1	51·1	1·29	13·5	12·6	0·18	6·99	11·3	2·31	0·05	0·14					99·5
39B	2	MSC	M1	51·2	1·57	12·7	13·9	0·24	6·50	11·3	2·46	0·08	0·17					100·1
40	6	MSC	B	52·1	1·10	15·0	11·0	0·16	5·92	10·7	2·60	0·18	0·16	1·366	0·061	0·155	0·004	100·5
41A	3	MSC	B	52·0	0·96	15·1	9·71	0·21	6·25	11·1	2·56	0·10	0·09	1·333	0·057	0·212	0·022	99·7
41B	2	MSC	M2	67·6	0·79	11·7	9·38	0·19	0·57	4·45	4·32	0·32	0·18	1·468	0·016	0·333	0·006	101·4
42A	2	MSC	M2	50·9	1·25	13·8	12·3	0·20	6·55	11·1	2·39	0·06	0·08	0·807	0·090	0·147	0·012	99·6
42B	1	MSC	M2	51·9	1·40	13·9	13·1	0·24	5·78	10·2	2·79	0·06	0·14					99·5
43A	1	MSC	M2	51·6	1·22	14·2	11·7	0·14	6·77	11·6	2·44	0·08	0·17					99·9
43B	2	MSC	M2	52·2	1·72	13·0	14·8	0·24	4·70	9·16	3·04	0·10	0·18	1·070	0·080	0·217	0·009	100·5
44	5	MSC	M2	51·3	1·22	14·0	12·4	0·21	6·89	11·3	2·33	0·05	0·17					99·9
45A	1	MSC	M2	51·3	1·75	13·3	15·1	0·25	4·65	9·34	2·69	0·13	0·23					98·7
45B	1	MSC	M2	51·6	1·46	13·6	13·3	0·18	6·38	11·1	2·38	0·04	0·16					100·1
45C	4	MSC	M2	65·7	0·77	11·4	10·5	0·22	0·39	4·73	4·02	0·32	0·24	1·738	0·064	0·271	0·006	100·3
46	5	MSC	M2	53·0	2·36	11·8	17·9	0·29	2·77	7·91	3·03	0·13	0·30	1·065	0·106	0·265	0·015	100·9
47	3	MSC	M2	51·1	1·83	13·0	15·4	0·21	5·47	9·85	2·81	0·10	0·31	0·507	0·144	0·179	0·021	101·0
BC-15	2	MSC	M1	51·4	1·40	13·7	13·0	0·22	6·33	10·8	2·38	0·05	0·13					99·5
BC-19	1	MSC	M2	51·7	1·56	13·6	13·9	0·25	5·27	9·72	2·49	0·07	0·17					98·7
2257		MSC	X	56·9	0·88	15·6	7·55	0·16	4·28	7·95	3·34	0·75	0·38					97·8
2261		MSC	B	52·3	1·53	13·7	13·2	0·21	4·72	9·23	2·99	0·14	0·17					98·3

Major element oxides by electron probe; H_2O, S, Cl and F by Knudsen cell mass spectrometry. Group, mean of all samples in group; *n*, number of individual samples averaged into mean; absolute error (wt %, 1σ) from mean for Group 16 is 0·42 (SiO_2), 0·04 (TiO_2), 0·13 (Al_2O_3), 0·22 (FeO*), 0·02 (MnO), 0·09 (MgO), 0·19 (CaO), 0·06 (Na_2O), 0·03 (K_2O) and 0·02 (P_2O_5); FeO*, total Fe as FeO. Settings: ER, East Manus Rifts; SR, Southern Rifts; Smt, Seamount; MSC, Manus Spreading Center; ETZ, Extensional Transform Zone. Types: A, arc; B, BABB; M, MORB; X, XBABB; E, 'enriched'; subtypes described in text.

Table 3: Isotopic data

Sample	Setting	Type	$^{87}Sr/^{86}Sr$	$^{143}Nd/^{144}Nd$	ε_{Nd}	$^{206}Pb/^{204}Pb$	$^{207}Pb/^{204}Pb$	$^{208}Pb/^{204}Pb$
14-5	ER	A1	0·703593 ± 12	0·513039 ± 6	7·6			
14-9	ER	A1				18·796	15·544	38·405
15-4	ER	A2	0·703719 ± 9	0·513034 ± 8	7·5			
16-14	ER	A2	0·703611 ± 9	0·513046 ± 6	7·7	18·744	15·541	38·383
17-1	ER	A2	0·703551 ± 10	0·513080 ± 6	8·4			
18-4	ER	Be	0·703438 ± 15	0·513021 ± 12	7·2	18·751	15·53	38·358
19-12	SR	Bs	0·703204 ± 10	0·513084 ± 5	8·5	18·780	15·527	38·366
21-2	SR	Bs	0·703387 ± 16	0·513080 ± 8	8·4			
22-2	SR	Bs	0·703420 ± 9					
23-2	Smt	Ms	0·703350 ± 13	0·512959 ± 10	6·0	18·525	15·505	38·327
23-4	Smt	Ms	0·703398 ± 16	0·512982 ± 10	6·5			
24-1	MSC	M1	0·703224 ± 12	0·513052 ± 5	7·8	18·127	15·479	37·988
24-9	MSC	X3	0·703248 ± 12	0·513066 ± 5	8·1			
25-2	MSC	M1	0·703302 ± 10	0·513053 ± 6	7·9			
28-1	MSC	B	0·703389 ± 13	0·513034 ± 7	7·5	18·437	15·509	38·175
32-5	ETZ	M1	0·703309 ± 13	0·513067 ± 8	8·1	17·983	15·466	37·891
33-3	ETZ	M1	0·703512 ± 14	0·513063 ± 5	8·1			
34-1	ETZ	B	0·703445 ± 13	0·513026 ± 10	7·3			
36-4	MSC	X2				18·740	15·531	38·317
38-4	MSC	M1	0·703234 ± 13	0·513086 ± 8	8·5			
39-1	MSC	M1				18·198	15·489	38·013
41-1	MSC	M2	0·703258 ± 13	0·513094 ± 6	8·7			
42-1	MSC	M2	0·703257 ± 14	0·513095 ± 7	8·7			
47-1	MSC	M2	0·703420	0·513063 ± 6	8·1			

All analyses by solid-source mass spectrometry at Australia National University. $^{87}Sr/^{86}Sr$ for NBS 987 = 0·710200 ± 10. $\varepsilon_{Nd} = (^{143}Nd/^{144}Nd)_{meas}/(^{143}Nd/^{144}Nd)_{CHUR}$, where $(^{143}Nd/^{144}Nd)_{CHUR} = 0{\cdot}51265$. Settings: ER, East Manus Rifts; SR, Southern Rifts; Smt, seamount; ETZ, Extensional Transform Zone; MSC, Manus Spreading Center. Types: A, arc; B, BABB; X, XBABB; M, MORB; subtypes discussed in the text.

Twenty-seven natural glasses were analyzed for the volatile components H_2O, CO_2, S, Cl and F (Table 2) at the University of Hawaii by methods described by Aggrey *et al.* (1988). Hand-picked glass chips, free of phenocrysts, were cleaned before analysis. The chips were then ignited in a Knudsen cell furnace coupled to a quadrupole mass spectrometer. Mass pyrograms of count rate vs temperature at individual masses were integrated to give concentrations. Twenty-two glasses have been analyzed for Sr, Nd and/or Pb isotopes (Table 3) using methods described by Woodhead *et al.* (1998). In addition, 24 glasses have been analyzed for He isotopes (Macpherson *et al.*, 1998). Nine glasses were analyzed for a range of trace elements using inductively coupled plasma-source mass spectrometry (ICP-MS) at the Australian National University (ANU) (Table 4).

Whole-rock major, minor and trace element analyses

Major, minor and trace elements were determined by X-ray fluorescence (XRF) spectrometry on 90 whole-rock *Moana Wave* samples using a fully automated Siemens spectrometer at ANU following methods similar to those of Norrish & Hutton (1977). Total iron was analyzed by XRF; FeO was measured by titration of excess ammonium metavanadate calibrated against $K_2Cr_2O_7$. For all major and minor elements, each sample was analyzed in duplicate and the resulting concentrations averaged. Estimated accuracy is ±1% relative. Trace elements were determined on pressed powder pellets using a fully automated Philips PW 1400 spectrometer at ANU, following methods described by Norrish & Hutton (1977) and Chappell (1992); Nb was determined by XRF at the University of Hawaii using an automated Siemens

Table 4: Glass trace element analyses by ICP-MS

Sample:	14-9	16-14	19-12	23-2	24-1	28-1	32-5	36-4	39-1
Group:	14A	16	19	23	24A	28A	32	36D	39A
Location:	ER	ER	SR	Smt	MSC	MSC	ETZ	MSC	MSC
Type:	A1	A2	Bs	Ms	M1	B	M1	X2	M1
Li	5·36	6·22	7·85	3·80	6·90	5·93	5·17	9·65	7·49
Be	0·45	0·56	0·36	0·19	0·47	0·38	0·34	0·83	0·46
Sc	35·93	32·32	36·7	48·1	46·9	43·37	42·50	27·01	45·62
V	363	275	331	257	415	362	306	270	423
Cr	22·53	106·94	76·18	412·7	173·61	334·64	279·0	79·52	86·09
Co	33·76	28·52	38·85	51·95	47·58	45·09	48·15	27·97	48·01
Ni	22·46	42·94	52·63	227·43	65·80	101·64	101·53	48·43	54·06
Cu	94·84	77·47	105·39	122·33	108·94	103·92	104·11	71·41	109·13
Zn	59·00	53·00	72·07	48·01	89·49	74·99	69·47	55·28	92·80
Ga	15·64	14·71	15·71	13·25	16·85	15·33	14·86	16·02	16·80
Rb	4·91	11·17	3·33	0·07	0·84	1·64	0·51	8·78	0·90
Sr	448	441	105	61·6	77·7	100·5	73·20	456	75·31
Y	13·41	14·89	25·96	24·43	36·60	29·62	26·60	18·42	38·46
Zr	31·41	45·23	52·60	32·30	72·13	55·35	51·14	94·70	73·49
Nb	0·47	0·75	0·69	0·23	1·45	1·09	0·87	4·93	1·25
Cs	0·23	0·33	0·100	0·002	0·014	0·035	0·007	0·365	0·018
Ba	121·16	173·50	32·89	1·235	9·126	19·44	5·173	191·8	10·93
La	2·865	4·757	2·088	0·756	2·149	2·015	1·422	16·526	2·191
Ce	6·912	11·048	5·823	2·899	7·415	6·351	5·131	31·790	7·460
Pr	1·026	1·564	0·956	0·555	1·345	1·103	0·949	3·572	1·356
Nd	5·284	7·609	5·443	3·476	8·060	6·44	5·780	13·885	8·090
Sm	1·557	2·077	2·011	1·467	3·061	2·409	2·247	2·739	3·088
Eu	0·593	0·691	0·793	0·627	1·123	0·913	0·856	0·863	1·129
Gd	1·828	2·233	2·964	2·420	4·405	3·501	3·233	2·672	4·524
Tb	0·333	0·382	0·589	0·511	0·874	0·702	0·640	0·472	0·896
Dy	2·015	2·276	3·761	3·491	5·550	4·460	4·077	2·839	5·738
Ho	0·452	0·504	0·879	0·839	1·255	1·018	0·916	0·620	1·318
Er	1·363	1·472	2·636	2·675	3·748	3·035	2·739	1·827	3·954
Yb	1·359	1·433	2·594	2·723	3·618	2·967	2·598	1·790	3·778
Lu	0·206	0·220	0·398	0·421	0·537	0·447	0·387	0·272	0·573
Hf	0·899	1·267	1·482	0·939	2·078	1·607	1·500	2·162	2·145
Ta	0·034	0·049	0·055	0·023	0·101	0·076	0·062	0·277	0·090
Pb	1·880	2·660	0·806	0·110	0·456	0·641	0·352	3·506	0·467
Th	0·272	0·272	0·155	0·024	0·112	0·138	0·071	3·107	0·119
U	0·143	0·274	0·274	0·008	0·035	0·052	0·020	1·069	0·040

All analyses by ICP-MS at Australia National University (analyses by Jon Woodhead).

spectrometer and an end-window Rh tube. Whole-rock XRF data for *Moana Wave* samples are presented in Table 5. Data for nine samples from the R.V. *Akademik Mstislav Keldysh* cruise have been presented by Sinton (1997).

Of the 90 samples analyzed by XRF, 38 were selected for analysis of REE, Sc, Cr, Cs, Hf, Th and U by instrumental neutron activation (INAA) at ANU using techniques similar to those of Goles (1977). INAA data are presented in Table 6.

ROCK CLASSIFICATION

A variety of chemical discriminants can be used to classify magma types within the Manus Basin. Those with the

Table 5: Whole-rock XRF data

Sample:	14-5	14-6	14-9	15-2	15-4	15-6	16-9	16-14	17-1	17-3	17-4	17-10	18-1	18-3	18-4
Group:	14B	14A	14A	15	15	15	16	16	17A	17A	17B	17A	18B	18A	18B
Type:	A1	A1	A1	A2	A2	A2	A2	A2	A2	A2	A2	A2	Be	Be	Be
Setting:	ER	ER	ER	ER	ER	ER	ER	ER	ER	ER	ER	ER	ER	ER	ER
SiO_2	61·53	52·01	52·92	52·95	52·73	53·13	53·73	54·13	64·11	63·31	66·45	61·85	52·29	51·36	52·50
TiO_2	0·79	0·56	0·60	0·38	0·38	0·36	0·57	0·56	0·84	0·82	0·72	0·82	0·52	0·44	0·51
Al_2O_3	14·44	16·59	16·13	13·67	13·71	12·50	15·78	15·71	14·87	14·31	13·95	14·41	16·46	16·50	16·49
Fe_2O_3	1·91	3·06	10·64	3·06	3·07	2·66	2·11	1·86	1·38	1·08	0·89	1·39	1·74	1·89	1·78
FeO	5·50	5·88		6·31	6·30	6·40	5·51	5·73	4·57	4·64	3·95	4·43	6·22	5·83	6·20
MnO	0·15	0·15	0·16	0·15	0·16	0·15	0·13	0·13	0·14	0·13	0·13	0·14	0·14	0·14	0·14
MgO	1·98	6·02	5·47	7·29	7·18	8·42	5·76	5·63	1·85	1·84	1·18	1·84	6·80	7·72	6·96
CaO	5·35	11·03	10·04	11·30	11·33	11·60	9·98	9·99	4·66	4·54	3·38	4·54	11·61	12·73	11·73
Na_2O	4·23	2·67	3·02	1·90	1·97	1·74	2·96	2·90	4·46	4·67	4·75	4·32	2·26	1·94	2·19
K_2O	1·11	0·43	0·46	0·90	0·98	0·80	0·78	0·76	1·44	1·31	1·66	1·58	0·32	0·27	0·32
P_2O_5	0·24	0·10	0·10	0·19	0·19	0·17	0·17	0·17	0·31	0·29	0·17	0·30	0·08	0·06	0·07
S	<0·02	<0·02	0·03	<0·02	<0·02	<0·02	0·05	0·04	<0·02	0·02	<0·02	<0·02	0·02	<0·02	<0·02
H_2O^+	1·76	0·84		1·05	1·39	1·06	1·27	1·35	1·86	1·73	1·63	2·50	1·00	0·62	0·90
H_2O^-	0·32	0·31		0·87	0·55	0·57	0·65	0·30	0·46	0·79	0·34	1·22	0·32	0·35	0·32
CO_2	0·30	0·33		0·39	0·49	0·43	0·49	0·49	0·28	0·51	0·36	0·27	0·33	0·32	0·58
Rest	0·17	0·15	0·17	0·19	0·18	0·19	0·16	0·16	0·12	0·13	0·12	0·12	0·12	0·13	0·12
	99·78	100·13	99·74	100·60	100·61	100·18	100·10	99·91	101·35	100·12	99·68	99·73	100·21	100·30	100·81
O = S			0·01				0·02	0·02		0·01					
Total	99·78	100·13	99·73	100·60	100·61	100·18	100·08	99·89	101·35	100·11	99·68	99·73	100·21	100·30	100·81
Trace elements (ppm)															
Sc	21	38			43		34	31	16		14				34
V	215	269	347	255	243	239	245	242	70	74	21	68	237	219	237
Cr	2	20	17	168	182	257	69	72	21	25	15	20	101	129	108
Co	18								13					42	
Ni	<1	28	21	39	39	57	39	40	15	15	5	14	65	76	64
Cu	181	94	113	95	89	98	82	85	26	30	17	26	91	86	93
Zn	76	68	74	71	60	67	68	55	74	91	90	87	69	50	66
Ga	15·0	14·5	13·5	10·0	11·5	9·0	14·5	14·5	16·0	14·0	15·5	15·5	14·0	12·5	14·0
Rb	13·0	4·0	5·0	13·0	13·0	13·0	10·5	10·0	19·0	19·5	24·0	19·5	3·5	3·0	3·5
Sr	444	449	452	565	540	505	443	436	342	355	306	345	181	202	183
Y	20	9	12	9	8	9	12	12	27	29	31	27	12	10	11
Zr	73	28	30	21	24	19	44	46	98	95	121	95	31	24	29
Nb	1·4	0·9	0·7	0·6	1·0	1·1	1·2	1·0	1·5	1·7	2·0	1·6	0·8	0·7	0·6
Ba	275	100	125	185	170	165	165	165	255	270	305	245	62	66	68
Pb	5	2	2	3	3	3	2	3	4	3	5	4	<1	1	2

lowest K_2O contents are tholeiitic with moderate to strong iron-enrichment trends (Figs 3 and 4). The mafic examples of the lowest-K suite are similar to MORB. A group of lavas that are mildly enriched in alkali elements and slightly depleted in high field strength, incompatible elements are similar to BABB from the Mariana Trough and elsewhere, and show trends subparallel to the MORB tholeiitic trend. One group from the Extensional Transform Zone (ETZ) (Group 31A) has many characteristics of MORB tholeiites but with relative enrichments in both lithophile and high field strength, incompatible elements, similar to transitional (T) MORB from oceanic spreading centers. Samples with higher K_2O contents show no Fe enrichment, similar to low- and medium-K lavas of the island arc association

Table 5: continued

Sample:	19-11	19-12	20-2	20-3	21-1	21-2	21-3	22-2	22-5	22-7	23-2	23-4	24-1	24-9	25-1
Group:	19	19	20	20	21	21	21	22A	22B	22B	23	23	24A	24B	25B
Type:	Bs	Bs	Bs	Bs	Bs	Bs	Bs	Bs	Bs′	Bs′	Ms	Ms	M1	X3	M1
Setting:	SR	SR	SR	SR	SR	SR	SR	SR	SR	SR	SMT	SMT	MSC	MSC	MSC
SiO_2	52·81	52·75	50·84	51·31	51·45	50·21	50·07	49·88	50·75	50·63	47·24	47·57	50·29	57·72	50·50
TiO_2	0·88	0·87	0·60	0·59	0·76	0·68	0·69	0·55	1·04	1·03	0·62	0·63	1·38	0·98	1·43
Al_2O_3	15·34	15·28	16·06	16·05	15·41	15·90	15·96	16·44	15·28	15·20	16·69	16·83	13·61	15·28	13·44
Fe_2O_3	2·03	1·98	1·22	1·11	1·97	1·94	2·41	2·02	1·70	1·87	1·22	1·43	1·91	1·67	2·27
FeO	7·98	8·00	6·34	6·49	7·66	6·60	6·13	5·82	7·93	7·78	8·10	7·87	10·68	6·19	10·87
MnO	0·17	0·16	0·14	0·14	0·17	0·15	0·14	0·14	0·16	0·17	0·17	0·17	0·20	0·13	0·21
MgO	5·97	5·84	7·70	7·79	6·98	8·35	7·88	8·63	7·56	7·39	10·72	9·89	6·73	3·59	6·46
CaO	10·46	10·34	12·68	12·79	11·71	12·35	12·44	12·57	11·92	11·93	12·44	12·66	11·45	7·33	10·90
Na_2O	2·61	2·65	2·11	2·16	2·26	2·23	2·15	2·21	2·45	2·47	2·10	2·04	2·46	3·89	2·52
K_2O	0·25	0·24	0·23	0·23	0·24	0·22	0·25	0·23	0·12	0·13	0·01	0·02	0·06	0·64	0·06
P_2O_5	0·09	0·09	0·08	0·08	0·09	0·08	0·09	0·08	0·09	0·09	0·03	0·04	0·12	0·20	0·12
S	0·07	0·09	0·04	0·04	0·06	0·06	0·10	0·06	0·11	0·11	0·06	0·06	0·15	0·03	0·16
H_2O^+	0·70	1·15	1·16	1·13	0·79	0·73	0·77	0·74	0·66	0·76	0·24	0·17	0·47	1·76	0·56
H_2O^-	0·27	0·36	0·26	0·20	0·31	0·32	0·38	0·34	0·21	0·24	0·11	0·11	0·12	0·38	0·19
CO_2	0·36	0·33	0·38	0·28	0·30	0·37	0·47	0·45	0·32	0·30	0·14	0·21	0·29	0·71	0·31
Rest	0·12	0·13	0·14	0·15	0·13	0·16	0·16	0·16	0·15	0·14	0·18	0·16	0·15	0·14	0·15
	100·11	100·26	99·98	100·54	100·27	100·30	100·09	100·30	100·45	100·24	100·07	99·86	100·07	100·64	100·15
O = S	0·03	0·04	0·02	0·02	0·03	0·03	0·05	0·03	0·05	0·05	0·03	0·03	0·07	0·01	0·08
Total	100·08	100·22	99·96	100·52	100·24	100·27	100·04	100·27	100·40	100·19	100·04	99·83	100·00	100·63	100·07
Trace elements (ppm)															
Sc		36	44		46	39		38	50		48	49	47	26	
V	298	306	230	237	292	247	246	218	299	293	238	234	381	253	398
Cr	54	51	224	256	33	257	251	263	180	188	358	302	126	21	90
Co		45		41		45		44				59		31	53
Ni	51	48	93	99	53	122	114	133	81	81	246	203	64	26	57
Cu	126	121	89	92	140	102	105	195	95	94	137	138	117	92	119
Zn	87	89	60	53	71	61	66	51	80	67	61	52	94	60	113
Ga	16·5	16·0	13·0	13·0	14·3	13·3	14·0	12·8	15·5	15·5	13·0	13·0	17·0	15·5	17·0
Rb	3·5	3·0	3·0	3·0	2·5	1·8	2·5	2·0	1·0	1·0	<0·5	<0·5	1·0	7·5	0·5
Sr	106	107	169	163	164	220	222	259	118	117	62	63	79	251	77
Y	21	21	14	14	18	16	15	12	21	22	21	21	31	19	30
Zr	52	53	33	31	38	33	33	25	59	55	34	34	73	100	76
Nb	1·1	0·9	0·6	0·5	0·5	0·7	1·0	0·5	0·8	0·7	0·6	0·4	1·6	4·0	1·4
Ba	34	28	40	40	36	37	36	42	12	14	4	<2	12	155	10
Pb	<1	<1	1	1	<1	<1	<1	<1	<1	<1	<1	<1	<1	3	<1

(Fig. 3). Within this group, we recognize three distinct magma types: low-K (A1) and medium-K (A2) arc magmas, and a strongly vesicular type from the MSC (extreme back-arc basin basalts; XBABB—see below).

THE MANUS BASIN

The Manus Basin forms the northeastern part of the Bismarck Sea. It is bounded on the SW by the Willaumez Rise, and on the north, east and south by the islands of Manus, New Hanover, New Ireland and New Britain (Fig. 1). According to the tectonic reconstruction of Falvey & Pritchard (1985), south-dipping subduction along the Manus Trench before ~10 Ma created a linear island arc now represented by parts of the Huon peninsula of Papua New Guinea, New Britain, Manus Island, New Hanover, New Ireland and the Solomon Islands. About 10 Ma, the Ontong Java Plateau collided with New Ireland and the North Solomon Arc, and subduction of the Pacific Plate

Sample:	25-2	26-5	26-14	27-5	28-1	29-3	29-4	30-1	30-2	30-3	31-1	31-3	31-8	32-3	32-5
Group:	25A	26	26	27	28A	29A	29B	30B	30A	30C	31A	31B	31C	32	32
Type:	M1	M1	M1	M1	B	M1	B	B	B	B	E	M1	B	M1	M1
Setting:	MSC	ETZ	ETZ	ETZ	MSC	ETZ	ETZ	ETZ	ETZ	ETZ	ETZ	ETZ	ETZ	ETZ	ETZ
SiO_2	50·18	50·64	50·74	50·17	50·38	49·58	51·21	53·58	53·01	58·64	50·24	50·40	51·44	49·81	49·63
TiO_2	0·95	1·03	1·06	1·07	1·05	0·96	0·70	1·29	1·05	1·14	1·46	1·19	0·35	0·99	0·98
Al_2O_3	14·98	14·32	14·45	14·64	14·35	14·92	15·89	14·71	15·41	12·61	14·30	13·80	15·23	15·46	14·84
Fe_2O_3	1·78	1·88	1·93	1·62	2·18	1·62	1·41	2·95	2·27	2·37	2·46	2·15	1·51	1·60	1·54
FeO	8·34	8·84	8·83	9·37	8·66	8·63	6·48	9·05	8·12	8·46	8·94	10·29	5·57	8·23	8·56
MnO	0·17	0·18	0·19	0·18	0·18	0·17	0·14	0·20	0·17	0·17	0·19	0·20	0·13	0·16	0·17
MgO	8·23	7·46	7·36	7·71	7·48	8·38	8·86	4·21	5·48	4·26	6·94	7·00	9·30	7·97	8·14
CaO	12·58	11·94	11·98	12·11	11·56	12·58	12·06	8·47	9·90	7·92	11·85	11·61	13·57	12·98	12·36
Na_2O	2·30	2·41	2·41	2·24	2·25	2·23	2·30	3·39	2·91	2·68	2·65	2·49	1·44	2·23	2·33
K_2O	0·08	0·09	0·13	0·05	0·15	0·04	0·14	0·31	0·27	0·17	0·22	0·05	0·08	0·07	0·05
P_2O_5	0·08	0·08	0·08	0·08	0·11	0·08	0·08	0·15	0·12	0·12	0·14	0·09	0·04	0·07	0·07
S	0·10	0·12	0·10	0·14	0·13	0·12	0·03	0·04	0·06	0·06	0·13	0·15	0·02	0·11	0·12
H_2O^+	0·29	0·54	0·45	0·26	0·56	0·38	0·65		0·80	0·90	0·41	0·32		0·27	0·41
H_2O^-	0·16	0·22	0·22	0·07	0·35	0·12	0·20		0·36	0·22	0·24	0·20		0·10	0·14
CO_2	0·24	0·25	0·27	0·16	0·33	0·27	0·25		0·33	0·29	0·25	0·40		0·23	0·31
Rest	0·14	0·12	0·13	0·14	0·16	0·15	0·16	0·13	0·12	0·12	0·14	0·13	0·14	0·15	0·14
	100·60	100·12	100·33	100·01	99·88	100·23	100·56	98·48	100·38	100·13	100·56	100·47	98·82	100·43	99·79
O = S	0·05	0·06	0·05	0·07	0·06	0·06	0·01	0·02	0·03	0·03	0·06	0·07	0·01	0·05	0·06
Total	100·55	100·06	100·28	99·94	99·82	100·17	100·55	98·46	100·35	100·10	100·50	100·40	98·81	100·38	99·73
Trace elements (ppm)															
Sc	43		50		44		39			32					42
V	272	315	324	310	327	269	214	361	310	360	330	345	223	271	276
Cr	257	59	52	204	233	272	281	2	8	3	105	42	370	326	197
Co						55									
Ni	107	66	66	93	99	118	158	9	19	11	56	51	135	98	102
Cu	106	117	110	114	113	115	80	37	65	48	91	130	74	105	120
Zn	67	84	84	73	90	83	64	105	90	98	75	100	54	78	82
Ga	14·5	15·0	15·5	14·5	15·5	14·5	13·5	15·5	17·0	13·5	16·5	16·0	8·5	12·5	12·5
Rb	1·0	1·0	1·5	0·5	1·5	<0·5	1·5	3·0	3·0	2·0	2·5	<0·5	1·0	0·5	0·5
Sr	78	80	81	71	101	72	171	175	175	137	109	68	87	81	75
Y	21	22	23	24	24	21	13	30	23	27	30	27	10	23	23
Zr	54	53	52	57	57	50	42	79	61	68	89	57	17	54	54
Nb	1·1	0·9	1·1	0·9	1·4	0·9	1·0	1·5	1·0	1·5	3·0	1·2	0·4	1·2	0·7
Ba	8	10	6	6	20	4	26	38	36	50	22	8	12	10	10
Pb	<1	<1	<1	<1	<1	<1	<1	2	1	2	1	<1	2	<1	<1

beneath this arc ended (Cooper & Taylor, 1987). At the same time, a counter-clockwise rotation of the New Ireland–North Solomon Arc and an associated subduction reversal occurred so that north-facing subduction began along the New Britain Trench. About 4 Ma, the composite New Britain–Huon Peninsula Arc rotated counter-clockwise to form the Bismarck Sea (Falvey & Pritchard, 1985).

In late 1985 and early 1986, the University of Hawaii conducted detailed SeaMARC II side-scan sonar and bathymetric surveys with associated seismic reflection, gravity and bottom-sampling programs using R.V. *Moana Wave* (Cruises 8517 and 8518) under the auspices of the Governments of the USA, Australia and New Zealand in cooperation with Committee for Coordination for Mineral

Table 5: continued

Sample:	33-1	33-2	33-3	33-5	33-9	34-1	35-1	35-2	35-3	35-3C	35-4	35-5	35-7	36-1	36-2
Group:	33B	33B	33A	33A	33B	34	35A	35A	35A	35C	35A	35A	35B	36B	36A
Type:	B	B	M1	M1	B	B	X1	X1	X1	Xc	X2	X1	X3	M1	M1
Setting:	ETZ	ETZ	ETZ	ETZ	ETZ	ETZ	MSC	MSC	MSC	MSC	MSC	MSC	MSC	MSC	MSC
SiO_2	52·44	52·30	50·69	49·63	52·28	50·02	55·79	55·60	56·59	53·13	54·41	55·71	56·72	51·62	49·94
TiO_2	1·27	1·27	0·97	0·97	1·24	0·88	0·77	0·77	0·78	0·63	0·88	0·81	0·91	1·23	0·95
Al_2O_3	14·68	14·64	14·38	14·44	14·58	14·73	15·83	15·92	16·20	17·33	15·89	16·35	15·67	13·56	14·72
Fe_2O_3	3·71	4·61	1·48	1·68	3·24	1·74	2·55	2·07	1·98	3·90	2·51	2·59	1·78	1·62	1·62
FeO	8·69	7·88	9·16	8·85	8·73	8·57	4·57	4·76	4·93	3·50	5·78	4·55	5·81	10·23	8·35
MnO	0·20	0·20	0·19	0·18	0·19	0·18	0·12	0·11	0·12	0·11	0·14	0·12	0·12	0·20	0·17
MgO	4·62	4·38	7·60	7·90	5·13	7·75	4·68	4·55	4·59	6·18	5·31	4·55	4·09	6·86	8·36
CaO	9·14	9·03	12·41	12·54	9·01	12·11	8·60	8·32	8·47	10·57	9·47	8·59	7·94	11·25	12·51
Na_2O	3·21	3·24	2·27	2·32	2·98	2·27	3·70	3·74	3·66	2·84	3·39	3·57	3·72	2·36	2·18
K_2O	0·29	0·39	0·04	0·07	0·46	0·08	0·73	0·70	0·70	0·50	0·58	0·73	0·66	0·06	0·05
P_2O_5	0·20	0·21	0·07	0·07	0·22	0·07	0·32	0·32	0·33	0·22	0·27	0·33	0·20	0·09	0·07
S	0·04	0·06	0·11	0·12	0·04	0·12	0·05	0·06	0·06	0·02	0·04	0·04	<0·02	0·13	0·11
H_2O^+	0·70	0·85	0·27	0·42		0·63					1·07	1·31	1·43		0·51
H_2O^-	0·25	0·46	0·07	0·16		0·19					0·37	0·47	0·65		0·22
CO_2	0·33	0·47	0·19	0·28		0·24					0·47	0·52	0·40		0·25
Rest	0·15	0·15	0·13	0·13	0·19	0·14	0·20	0·19	0·20	0·21	0·18	0·20	0·15	0·14	0·16
	99·92	100·14	100·03	99·76	98·29	99·72	97·91	97·11	98·61	99·14	100·76	100·44	100·25	99·35	100·17
O = S	0·02	0·03	0·05	0·06	0·02	0·06	0·02	0·03	0·03	0·01	0·02	0·02		0·06	0·05
Total	99·90	100·11	99·98	99·70	98·27	99·66	97·89	97·08	98·58	99·13	100·74	100·42	100·25	99·29	100·12
Trace elements (ppm)															
Sc			46			43	26						26		43
V	418	400	309	309	410	290	238	232	249	241	271	238	250	388	292
Cr	4	3	119	114	49	172	57	46	49	54	63	48	33	78	287
Co	43										36				
Ni	12	11	80	77	17	89	36	36	37	56	47	36	33	60	115
Cu	57	56	148	148	59	115	88	87	85	56	94	82	73	132	121
Zn	89	87	84	83	110	71	62	61	64	51	59	64	54	103	80
Ga	18·0	17·0	13·0	12·5	15·0	14·5	13·5	13·5	14·0	14·5	16·5	16·0	15·5	14·0	15·0
Rb	3·5	4·5	1·0	0·5	10·5	1·0	9·5	9·5	10·0	7·0	7·5	9·5	8·0	0·5	0·5
Sr	245	250	73	81	255	103	640	635	650	815	481	640	323	75	73
Y	27	28	24	24	30	19	16	16	16	9	18	14	19	30	21
Zr	79	80	50	50	88	42	121	123	127	85	106	128	91	67	48
Nb	1·9	2·1	0·7	0·9	2·0	0·7	6·1	6·1	6·8	3·5	4·8	6·5	3·9	1·0	1·0
Ba	72	74	12	14	300	18	235	230	250	200	175	235	175	20	12
Pb	2	2	1	<1	3	<1	5	4	5	4	3	5	3	1	<1

Resources in South Pacific Offshore Areas (CCOP/SOPAC). The survey mapping results have been reported by Taylor *et al.* (1991, 1994) and are summarized in Fig. 2. This region also has been mapped with multibeam bathymetry and explored using submersibles by Auzende *et al.* (2000). Volcanism associated with extension occurs along a series of rifts and spreading centers between three major, left-stepping, left-lateral transform faults (Taylor, 1979; Taylor *et al.*, 1991; Martinez & Taylor, 1996). Overall a transtensional tectonic regime dominates the fabric and kinematics of the region (Taylor *et al.*, 1994).

East Manus Rifts

In the eastern Manus Basin, ancient forearc crust is being stretched between the Weitin and Djaul Trans-

Sample:	36-4	36-6	36-8	37-1	37-2	38-3	38-4	38-8	38-9	39-1	39-2	40-1	40-6	41-1	41-3
Group:	36D	36D	36C	37	37	38A	38A	38B	38C	39A	39B	40	40	41B	41A
Type:	X2	X2	M1	M1	M1	M1	M1	B	B	M1	M1	B	B	M2	B
Setting:	MSC	MSC	MSC	MSC	MSC	MSC	MSC	MSC	MSC	MSC	MSC	MSC	MSC	MSC	MSC
SiO_2	54·71	56·12	51·11	50·73	50·35	50·68	50·91	51·31	52·86	50·46	51·09	51·51	51·76	66·75	52·19
TiO_2	0·81	0·82	1·98	1·22	1·24	1·37	1·38	1·17	1·22	1·23	1·39	1·07	1·08	0·79	0·93
Al_2O_3	16·26	16·08	13·18	13·94	13·98	13·38	13·41	14·28	14·01	13·70	13·45	14·72	14·85	11·25	15·17
Fe_2O_3	1·80	1·84	2·44	1·55	2·17	1·89	2·39	2·66	2·55	2·00	2·22	2·57	2·95	1·31	2·50
FeO	5·48	5·36	12·02	10·29	9·87	11·05	10·68	9·29	9·43	10·18	10·84	8·34	7·81	8·02	7·09
MnO	0·12	0·12	0·22	0·20	0·20	0·21	0·21	0·19	0·19	0·20	0·21	0·18	0·18	0·17	0·16
MgO	4·75	4·85	5·05	7·33	7·53	6·42	6·51	5·83	5·57	6·99	6·51	6·09	5·95	0·61	6·51
CaO	8·73	8·80	9·82	11·66	11·56	10·91	10·98	10·26	9·94	11·46	10·98	10·79	11·05	4·45	11·36
Na_2O	3·35	3·49	2·83	2·36	2·42	2·53	2·53	2·73	2·77	2·42	2·51	2·63	2·61	4·27	2·69
K_2O	0·65	0·67	0·10	0·05	0·05	0·06	0·06	0·22	0·26	0·05	0·06	0·23	0·26	0·31	0·18
P_2O_5	0·24	0·24	0·20	0·10	0·10	0·10	0·11	0·12	0·12	0·09	0·11	0·11	0·12	0·20	0·09
S	0·03	0·03	0·19	0·14	0·16	0·16	0·16	0·17	0·09	0·14	0·16	0·09	0·05	0·06	0·07
H_2O^+	1·67		0·79	0·42	0·22	0·42	0·44	0·99		0·47	0·22	1·07	0·85	1·50	0·76
H_2O^-	0·41		0·07	0·07	0·16	0·08	0·19	0·41		0·16	0·12	0·33	0·42	0·04	0·40
CO_2	0·40		0·32	0·19	0·43	0·30	0·33	0·49		0·30	0·23	0·44	0·30	0·32	0·43
Rest	0·17	0·17	0·15	0·14	0·15	0·14	0·14	0·14	0·14	0·14	0·15	0·14	0·14	0·11	0·14
	99·58	98·59	100·47	100·39	100·59	99·70	100·43	100·26	99·15	99·99	100·25	100·31	100·38	100·16	100·67
O = S	0·01	0·01	0·09	0·07	0·08	0·08	0·08	0·08	0·04	0·07	0·08	0·04	0·02	0·03	0·03
Total	99·57	98·58	100·38	100·32	100·51	99·62	100·35	100·18	99·11	99·92	100·17	100·27	100·36	100·13	100·64
Trace elements (ppm)															
Sc	31	26		46	46	47	48			47		40		15	40
V	240	250	436	355	347	392	397	368	398	369	391	341	343	26	304
Cr	52	57	59	149	124	84	86	11	6	81	84	65	63	6	127
Co								47			55				
Ni	43	48	40	75	79	51	54	38	35	58	55	55	52	1	79
Cu	72	81	88	118	116	117	118	112	102	128	120	117	118	14	120
Zn	64	64	114	83	95	91	97	101	103	102	94	91	93	152	61
Ga	15·5	14·0	17·5	15·5	16·5	16·5	16·5	16·5	15·0	16·5	16·5	16·5	16·0	22·5	14·5
Rb	8·5	9·0	1·5	1·0	0·5	0·5	0·5	2·0	3·0	0·5	0·5	2·5	2·5	4·0	1·5
Sr	441	462	76	71	74	71	72	130	134	71	71	161	165	88	157
Y	15	16	47	27	26	31	31	28	30	28	31	24	24	115	20
Zr	94	95	125	64	66	74	74	64	67	64	75	57	61	380	49
Nb	5·0	4·9	2·3	1·3	1·2	1·1	1·6	1·2	1·2	0·9	1·3	1·0	1·2	4·8	1·1
Ba	175	190	26	8	12	6	10	28	40	10	8	30	36	54	18
Pb	3	3	1	1	<1	<1	<1	<1	2	<1	<1	1	1	1	1

forms (Fig. 1); volcanism occurs in the associated pull-apart basin along a series of en echelon, sinuous rifts (i.e. Eastern Rifts or ER, Fig. 2a). These rifts are physiographic ridges rising to water depths <2000 m. The extent of lava fields and high sonar reflectivity associated with these ridges indicates that the area is moderately active volcanically, but the lack of well-defined magnetic anomalies and linear tectonic fabric suggests that rifting and/or seafloor spreading in this region is poorly organized.

High-SiO_2 lavas (andesites and dacites) were recovered from the easternmost ridge near 152°10′E, and from one of a cluster of domes between 151°30′ and 151°40′E (Fig. 2a). Lavas contained in the easternmost dredge (14) define the low-K, A1 type of Manus Basin arc magmas. Several seamounts have been recently active east of about

Table 5: continued

Sample:	41-4	41-7	42-1	42-3	43-1	44-1	45-1	45-2	45-3	45-4	45-6	46-2	47-1	BC15-1	BC19-1
Group:	41A	41B	42B	42A	43B	44	45B	45A	45C	45C	45C	46	47	BC15	BC19
Type:	B	M2	M2	M2	M2	M2	M2	M2	M2	M2	M2	M2	M2	M1	M2
Setting:	MSC	MSC	MSC	MSC	MSC	MSC	MSC	MSC	MSC	MSC	MSC	MSC	MSC	MSC	MSC
SiO_2	51·48	65·94	51·38	52·06	52·28	54·49	50·60	50·85	61·36	63·38	64·18	51·57	50·67	50·46	51·20
TiO_2	0·91	0·81	1·27	1·24	1·65	1·08	1·18	1·81	1·07	1·05	0·89	2·41	1·72	1·42	1·44
Al_2O_3	15·02	11·34	13·91	13·66	12·91	12·82	13·71	12·83	10·58	10·91	10·39	11·28	13·01	13·27	13·04
Fe_2O_3	2·19	0·86	2·73	2·32	2·85	1·67	1·84	3·36		1·13	0·71	3·18	2·94	2·15	2·45
FeO	7·30	8·55	9·56	9·56	11·54	9·27	10·03	11·75	11·64	10·20	9·77	14·65	11·79	10·90	11·11
MnO	0·16	0·18	0·20	0·19	0·23	0·18	0·20	0·23	0·21	0·22	0·20	0·27	0·37	0·21	0·22
MgO	6·73	0·62	6·27	6·65	4·90	6·73	7·16	4·75	1·59	0·58	0·51	2·85	5·43	6·44	5·47
CaO	11·27	4·59	10·87	11·20	9·36	10·69	11·63	9·38	5·93	5·04	4·49	8·02	10·20	10·81	9·82
Na_2O	2·63	4·26	2·61	2·44	3·00	2·14	2·28	2·79	3·48	4·00	3·88	3·11	2·72	2·41	2·59
K_2O	0·17	0·29	0·10	0·07	0·14	0·04	0·05	0·20	0·24	0·46	0·31	0·27	0·10	0·06	0·10
P_2O_5	0·09	0·19	0·11	0·10	0·15	0·08	0·09	0·19	0·29	0·32	0·26	0·31	0·17	0·11	0·13
S	0·06	0·05	0·15	0·14	0·16	0·12	0·13	0·17	0·10	0·11	0·06	0·21	0·19	0·15	0·15
H_2O^+	0·89	1·29	0·66		0·78			0·83		1·90		0·86	0·79		
H_2O^-	0·40	0·06	0·28		0·30			0·51		0·38		0·43	0·10		
CO_2	0·43	0·28	0·34		0·43			0·38		0·40		0·53	0·26		
Rest	0·15	0·11	0·14	0·14	0·15	0·13	0·14	0·15	0·12	0·11	0·12	0·12	0·16	0·15	0·14
	99·88	99·42	100·58	99·77	100·83	99·44	99·04	100·18	96·61	100·19	95·77	100·07	100·62	98·54	97·86
O = S	0·03	0·02	0·07	0·07	0·08	0·06	0·06	0·08	0·05	0·05	0·03	0·10	0·09	0·07	0·07
Total	99·85	99·40	100·51	99·70	100·75	99·38	98·98	100·10	96·56	100·14	95·74	99·97	100·53	98·47	97·79
Trace elements (ppm)															
Sc	43		45	46	45	43	46	42				42	45		
V	305	27	382	389	440	345	363	442	64	9	6	280	434	422	426
Cr	118	5	47	63	16	88	97	16	16	3	1	5	76	95	25
Co										12					
Ni	79	<1	52	58	30	65	67	30	9	<1	<1	5	54	59	42
Cu	111	14	123	130	100	130	123	78	55	13	15	44	103	118	115
Zn	79	146	85	100	108	90	98	140	182	172	199	158	114	110	123
Ga	15·5	21·5	16·0	14·0	18·5	12·5	13·5	18·5	18·5	22·5	20·0	22·0	17·0	15·0	15·0
Rb	1·5	4·0	1·0	1·0	1·5	0·5	0·5	2·0	3·0	5·0	4·5	2·5	1·5	0·5	1·0
Sr	163	92	98	89	83	72	72	90	89	92	90	83	87	77	82
Y	19	108	28	29	42	26	29	41	95	110	118	67	40	33	38
Zr	52	356	66	67	106	56	63	108	302	370	401	163	100	76	89
Nb	1·0	5·1	1·4	1·2	2·1	1·3	1·2	1·8	4·4	5·0	5·1	2·9	2·0	<0·5	1·0
Ba	20	48	14	18	26	18	18	22	56	54	56	24	22	10	8
Pb	<1	2	2	<1	1	1	<1	<1	1	2	3	2	2	1	2

A1, East Manus, low-K arc-type; A2, East Manus arc-type; Be, East Manus BABB; Bs, Southern Rift BABB; Bs′, low-K_2O type; M, MORB; B, BABB; X, XBABB; E, enriched; subtypes Ms, M1 are described in text.

151°55′E; we sampled one of these near 152°E (Fig. 2), which contained highly vesicular, olivine- and clinopyroxene-phyric basalts. Dredge 16 is from the inside of a small collapse structure about 2 km wide by 50 m deep; this feature has been shown to be the site of vigorously active hydrothermal venting (Binns & Scott, 1993). Dredge 18 was located on a low ridge on the NW side of the province (Fig. 2a). Samples from this dredge are BABB (type Be), generally similar chemically and isotopically to samples from the rift graben to the west.

Table 6: INAA analyses of Manus Basin lavas

Sample	Type	Sc	Cr	Cs	Hf	Th	U	La	Ce	Nd	Sm	Eu	Gd	Ho	Yb	Lu
East Manus																
14-5	A1	21	<1	0·4	1·6	3	<1	7·0	16·5	11	3·35	1·08	3·4	0·75	2·35	0·36
15-4	A2	43	199	0·2	0·5	2	2	4·2	8·6		1·74	0·56	1·6	0·30	0·99	0·17
16-14	A2	31	79	0·2	1·0			4·7	10·7		2·10	0·70	2·0	0·50	1·50	0·23
17-1	A2	16	25	0·4	2·2	4	<1	8·9	21·5	15	4·15	1·36	4·5	1·15	3·30	0·49
17-4	A2	14	15	0·5	2·9	5	1	10·0	24·5	16	4·75	1·40	4·7	1·15	3·85	0·57
18-4	Be	34	118	<0·1	0·7	3	1	2·0	5·0		1·38	0·50	1·6		1·56	0·24
Southern Rifts																
19-12	Bs	36	55	<0·1	1·2	3	<1	2·0	5·8		2·00	0·77	2·7	0·80	2·55	0·41
21-2	Bs	39	273	<0·1	0·7	2	<1	1·70	5·0		1·75	0·68	2·2		1·86	0·31
22-2	Bs	38	286	<0·1	0·6	3	<1	1·80	4·4		1·47	0·58	1·8		1·53	0·23
Seamount																
23-2	M1	48	375	<0·1	0·7	3	<1	0·85	2·7		1·48	0·63	2·2	0·75	2·75	0·46
23-4	M1	49	315	<0·1	0·7	3	<1	0·80	2·8		1·47	0·63	2·2	0·75	2·75	0·47
Extensional Transform Zone																
30-3	B	32	2	<0·1	1·4	3	1	4·0	9·8		2·70	0·96	3·4	1·05	3·05	0·44
32-5	M1	42	198	<0·1	1·1	2	1	1·40	4·2		2·15	0·82	3·0	0·80	2·60	0·40
33-3	M1	46	115	<0·1	1·0	2	<1	1·30	4·6		2·15	0·82	2·9	1·00	2·65	0·44
34-1	B	43	177	<0·1	1·0	3	1	1·65	5·0		2·00	0·79	2·7	0·75	2·45	0·39
Manus Spreading Center																
24-1	M1	47	125	<0·1	1·5	2	<1	2·2	7·0		3·10	1·09	3·9	1·20	3·60	0·59
24-9	X3	26	21	0·2	1·8	4	1	12·0	23·5	10·0	2·75	0·89	3·0	0·70	2·35	0·37
25-2	M1	43	260	<0·1	1·1	2	<1	1·50	4·8		2·20	0·81	3·0	0·90	2·65	0·41
28-1	B	44	240	<0·1	1·2	3	<1	1·95	5·7		2·40	0·92	3·4	0·90	2·95	0·48
35-1	X1	26	59	0·3	2·1	4	1	21·5	43·5	18	3·40	0·94	2·7	0·60	1·80	0·28
35-7	X3	26	35	0·3	1·7	4	2	12·1	23·0	9·6	2·60	0·83	2·6	0·75	2·30	0·34
36-2	M1	43	293	<0·1	1·0	3	<1	1·65	5·0		2·10	0·80	2·9	0·80	2·50	0·40
36-6	X2	26	54	0·3	1·7	4	2	15·7	31·0	12	2·70	0·86	2·5	0·65	1·80	0·28
37-1	M1	46	150	<0·1	1·4	2	<1	1·85	5·7		2·70	0·97	3·6	1·05	3·30	0·52
38-3	M1	47	82	<0·1	1·6	2	<1	2·1	6·5		3·00	1·10	4·2	1·10	3·75	0·59
38-4	M1	48	83	<0·1	1·5	2	<1	2·0	6·9		3·05	1·10	4·1	1·25	3·75	0·60
39-1	M1	47	78	<0·1	0·7	2	<1	1·80	5·9		2·75	1·03	3·7	1·10	3·25	0·54
40-1	B	40	63	<0·1	1·3	3	<1	2·6	7·2		2·60	0·96	3·4	0·85	3·05	0·47
41-1	M2	15	2	<0·1	9·0	3	<1	10·1	33·5	33	12·1	3·5	16	4·1	14·6	2·05
41-3	B	40	133	<0·1	1·0	<2	<1	2·1	6·1		2·10	0·74	2·6	0·75	2·50	0·40
42-1	M2	45	47	<0·1	1·4	<2	<1	2·1	6·5		2·80	1·01	3·8	1·00	3·45	0·53
42-3	M2	46	63	<0·1	1·3	2	1	2·0	6·3		2·70	0·99	3·7	0·95	3·15	0·51
43-1	M2	45	15	<0·1	2·4	2	1	3·3	10·4	8·5	4·20	1·42	5·5	1·60	5·30	0·78
44-1	M2	43	88	<0·1	1·2	2	<1	1·75	5·3		2·35	0·87	3·3	0·95	2·95	0·47
45-1	M2	46	98	<0·1	1·3	2	<1	1·65	5·5		2·60	0·97	3·6	1·10	3·20	0·51
45-2	M2	42	15	<0·1	2·4	4	<1	3·4	10·8	9·5	4·50	1·57	5·9	1·70	5·10	0·81
46-2	M2	42	2	<0·1	3·6	2	2	4·9	15·5	15	6·8	2·25	9·0	2·5	8·1	1·22
47-1	M2	45	79	<0·1	2·2	2	1	3·4	9·9		4·15	1·37	5·4	1·50	5·1	0·77

Types: A, arc; M, MORB; B, BABB; X, XBABB; see text for subtypes A1, A2, etc.

Southern Rifts

West of the Djaul Transform in the southern part of the Manus Basin, extension is occurring in two overlapping rift graben with axial lava flows referred to as the Southern Rifts (SR) (Fig. 1). The deep basins (2045–2635 m) and lack of extensive lava fields indicate that the SR have a

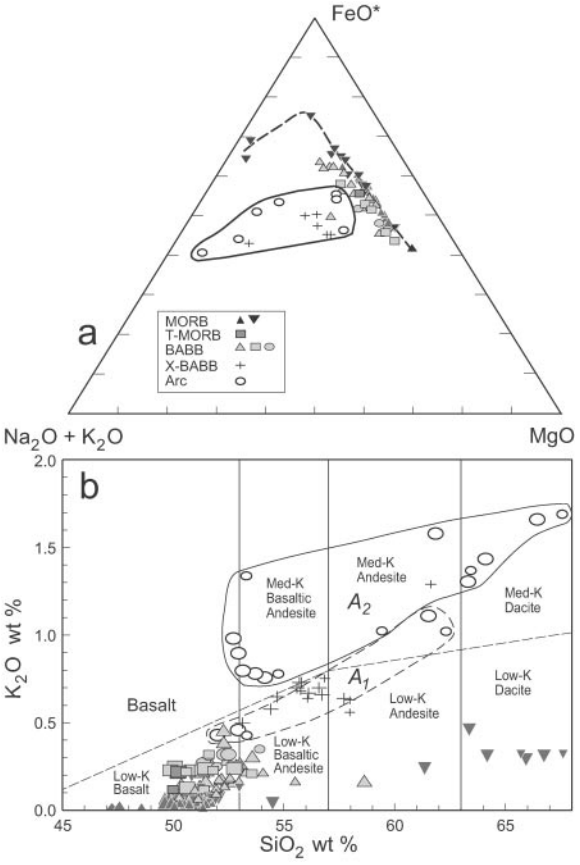

Fig. 3. AFM vs SiO_2 (wt %) (a) and K_2O vs SiO_2 (wt %) (b) for Manus Basin magmas. MORB and BABB lavas generally follow a tholeiitic iron-enrichment trend. It should be noted that non-basaltic differentiates of MORB are here included with MORB. Arc and XBABB lavas show no iron enrichment with progressive differentiation. The classification scheme in the lower figure is from Gill (1981). The division of arc lavas into low-K (A1) and medium-K (A2) types should be noted.

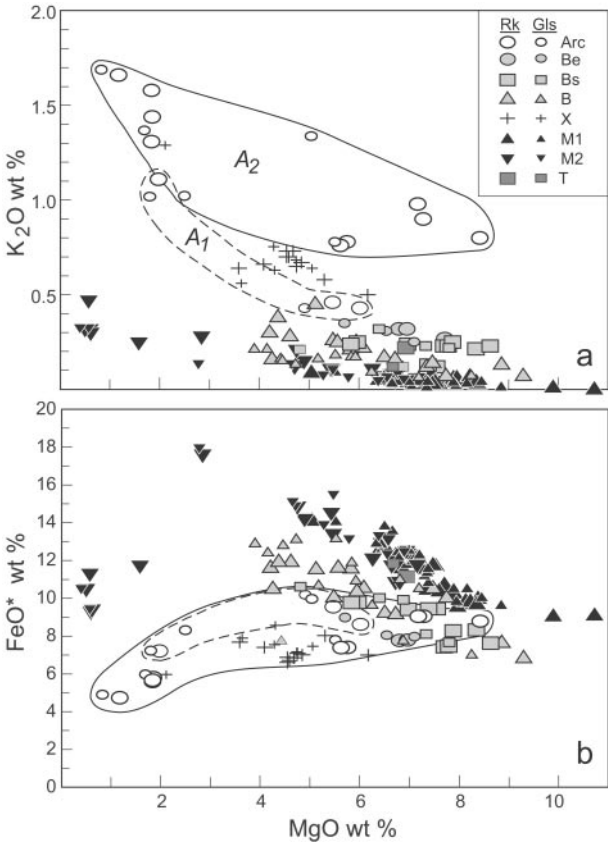

Fig. 4. K_2O vs MgO (a) and FeO* (total Fe as FeO) vs MgO (b) for Manus Basin lavas. Glass data (Gls) are plotted with smaller symbols than whole-rock (Rk) data (see legend). Legend notation as follows: ovals, arc lavas; types A1 and A2 are enclosed in dashed and continuous lines, respectively; Be, BABB from the ER; Bs, BABB from the SR; B, BABB from the MSC and ETZ; X, XBABB from the MSC. M1 and M2 are MORB (including differentiates ranging up to dacite compositions derived from MORB parents) from SW and NE of 150°08′E, respectively, on the MSC (see Fig. 2); T, dredge 31 T-MORB.

low magmatic budget. We obtained four dredge hauls from the SR, one from the eastern rift graben and three from the axis of the western graben. All collected samples are basaltic (Tables 2 and 5) with relatively low TiO_2. Those in dredge 19, the easternmost dredge, are moderately high-SiO_2 basalts. Dredge 22 contains some relatively low-K_2O BABB lavas, a characteristic generally more similar to BABB from the MSC and ETZ. On most variation diagrams the other SR samples (Bs) show slight enrichments in large ion lithophile elements (LILE: K, Rb, Sr, Ba) and H_2O (Figs 4–6) compared with BABB from the MSC and ETZ. In these respects Bs lavas are intermediate in composition between ER arc lavas and spreading center BABB.

Manus Spreading Center

The dominant extensional and volcanic feature in the Manus Basin is the 120 km long Manus Spreading Center (MSC), which strikes oblique to its bounding transforms, the Djaul Transform to the north and the Willaumez Transform to the south (Fig. 1). A minimum full spreading rate of 92 mm/yr in the south decreases progressively to the NE (Taylor *et al.*, 1994; Martinez & Taylor, 1996). This gradient is accompanied by a progressive change in morphology; the ridge axis is a topographic high rising to ~1950 m near 3°30′S, 149°55′E. Near 3°25′S, 150°00′E the cross-axis profile is very flat at a depth of ~2200 m; to the NE the axis evolves to a progressively wider and deeper axial valley, culminating at a maximum depth of ~2600 m near 3°05′S, 150°25′E. On the basis of the relative reflectivity on side-scan sonar records, the amount of recently erupted lava also increases from NE to SW, along with the progressive change in bathymetry and morphology. Taken together, these relations indicate

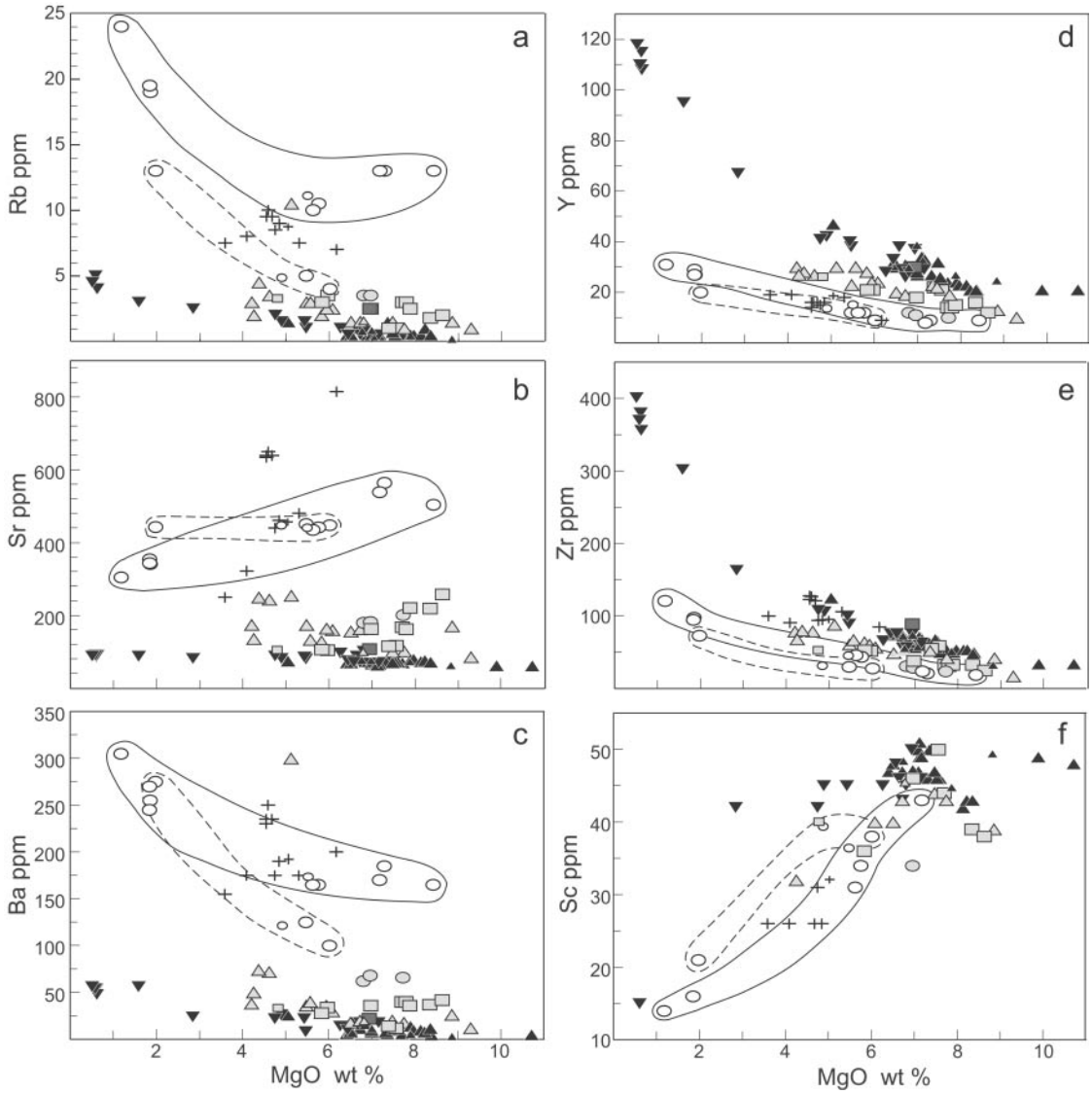

Fig. 5. Selected trace element variations vs MgO for Manus Basin lavas. Symbols as in Fig. 4.

an increase in magmatic budget from NE to SW along the MSC.

MORB lavas were recovered from nearly every dredge taken from the axis of the MSC. The exceptions are dredge 28, from the southernmost tip, which contained only BABB, and dredge 35 from the shallowest point on the MSC, which contained only XBABB (Fig. 2b). The flow sampled in dredge 28 is among the most reflective on side-scan records, suggesting that it may be one of the youngest lava flows in the entire area. For dredges in which both MORB and XBABB lavas were recovered (24, 36), the XBABB lavas appear to be extremely fresh and apparently younger. Data from subsequent bathymetric surveys and camera tow data (Tufar, 1989), indicate that the MSC above ~2200 m depth can be interpreted as a young XBABB volcano extending from near 150°46′E to about 150°49′E.

MORB also were absent from dredge 40, which was taken slightly off-axis near 150°08′E where the axis bends progressively more easterly; only BABB were recovered in this dredge. The sole rock recovered from camera run BC15 is BABB; this run crossed the axis and the exact location of the sample inadvertently collected during this station is not precisely known. The interpretation we make from these results is that the youngest lavas erupted along the MSC axis are MORB everywhere except along the MSC high, where the youngest lavas are XBABB, and on the southern tip, where BABB were recovered. Slightly older lavas, at least north of the axis between 150°02′ and 150°14′E, are BABB. The interpretation

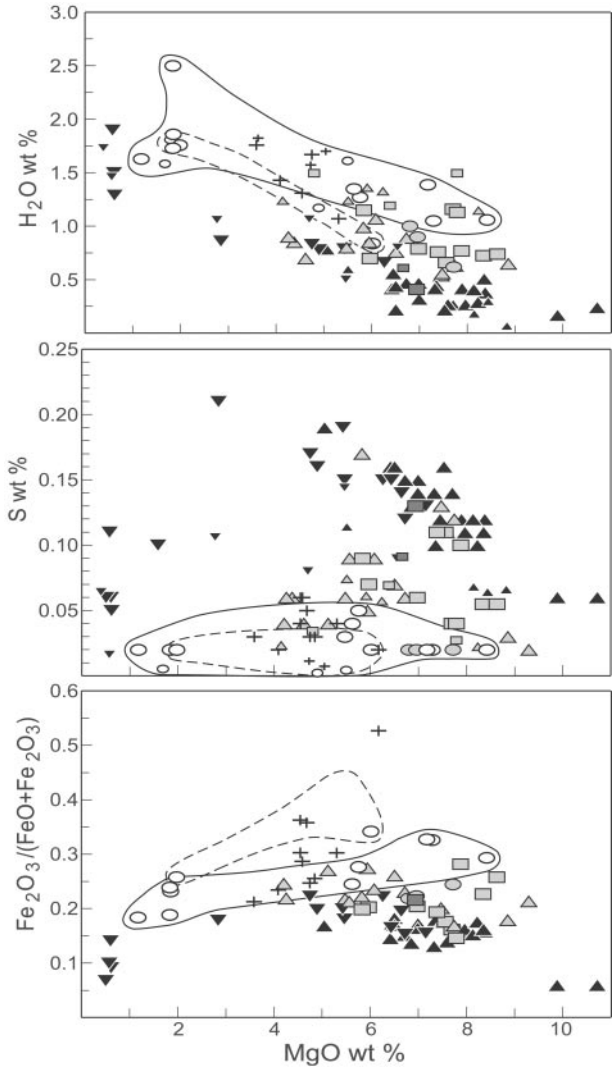

Fig. 6. H_2O, S and $Fe_2O_3/(FeO + Fe_2O_3)$ vs MgO for Manus Basin lavas. Symbols as in Fig. 4.

that axial MORB are younger than near-axis BABB has been confirmed by submersible observations near 150°02′E (Sinton, 1997).

The region near 150°08′E (dashed line on Fig. 2) marks a boundary in MORB magmatic composition; those to the NE (type M2) are enriched in H_2O and Sr, and are more differentiated than those to the SW. Because MORB Sr concentrations are little affected by fractionation (Fig. 5), the difference in Sr north and south of this boundary can be taken as a difference in primary magma composition. Lavas SW of 150°08′E average 74 $\pm$ 3 (1σ) ppm Sr, whereas those to the north average 86 $\pm$ 7 ppm. Hence, the MSC can be considered to consist of two magmatic segments, with a segment boundary near 150°08′E.

Most MSC MORB are ferrobasalts with ~12 wt % FeO*. However, there is a progressive increase in average degree of differentiation from near the MSC high, culminating in the highly variable ferrobasalts, andesites and dacites of dredge 45 near the NE tip, a geochemical pattern identical to that of oceanic propagating rifts (Sinton *et al.*, 1983). The MSC also shows similarities to propagating rifts at an even larger scale, including a V-shaped wake of young seafloor and an along-axis bathymetric gradient (see Hey *et al.*, 1989). However, interpretation of magnetic anomaly data over the MSC suggests that, rather than progressive rift propagation at more or less constant spreading rate, the MSC represents a spreading center with a gradient in spreading rate, decreasing to zero near the NE tip (Martinez & Taylor, 1996).

Seamount (RD-23)

One dredge was taken on a young flow emanating from the base of a large seamount just west of 150°00′E (Fig. 2a). Only one chemical group is represented in this dredge; it is a high-alumina basalt with the lowest SiO_2, and highest MgO, Ni and Cr of all the samples in this study. It has very low LILE concentrations and is strongly depleted in light REE (LREE); it is generally similar to highly depleted MORB and near-ridge seamount basalts, although it has the highest Pb isotope ratios of any MORB lava in the Manus Basin (Fig. 7).

Extensional Transform Zone

The ETZ (Fig. 1) is an oblique zone of right-stepping, overlapping, en echelon rifts between the Manus Spreading Center and the Willaumez Transform (Taylor *et al.*, 1994). MORB, BABB and the enriched lava of Group 31A were collected from the ETZ. The relationships between magma types and structure and age are far less systematic in the ETZ than elsewhere in the basin. On the basis of side-scan reflectivity, the youngest flow appears to be that sampled in dredge 27, which contained only MORB lavas. BABB lavas were recovered only from the eastern half of the ETZ, including targets on the shallowest part. The enriched lava type recovered in dredge 31 is enigmatic, although we note that this site is relatively close to a lava field between 3°30′ and 3°45′S that may be related to the Willaumez Rise. Lavas with ocean island affinity have been described from the St. Andrew Strait and Witu Islands (Fig. 1) on the Willaumez Rise (Johnson & Arculus, 1978; Johnson *et al.*, 1978).

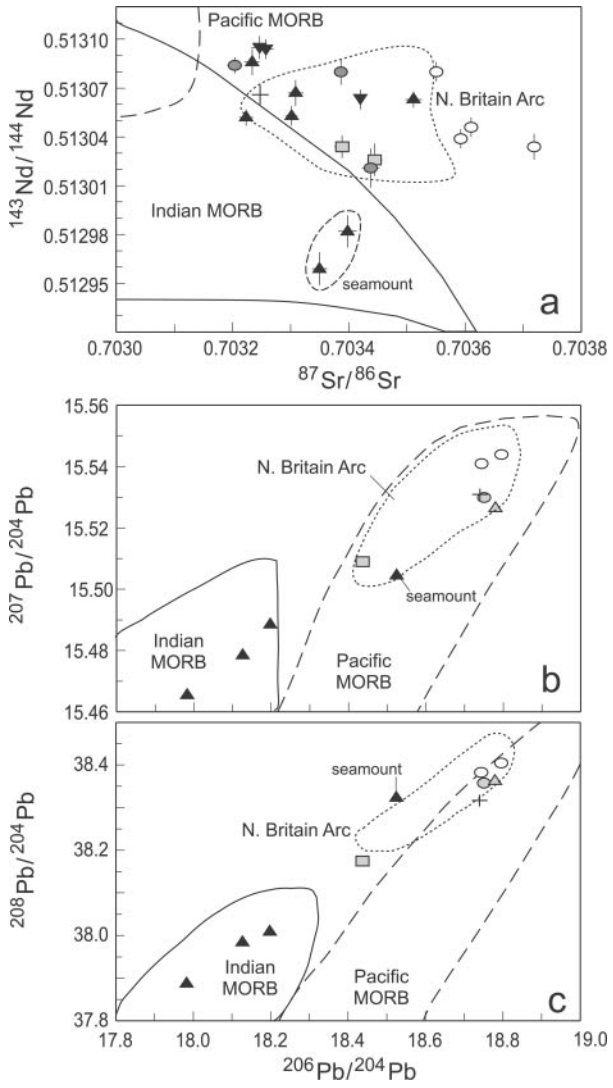

Fig. 7. Selected isotopic ratios for Manus Basin glasses. The fields for Pacific MORB, Indian MORB and the New Britain island arc are after Woodhead *et al.* (1998). Arc lavas from the ER have higher $^{87}Sr/^{86}Sr$ than any other lavas from the region, including those from the New Britain arc. Manus Basin MORB have Pb isotopic compositions typical of Indian Ocean MORB, and not of Pacific MORB.

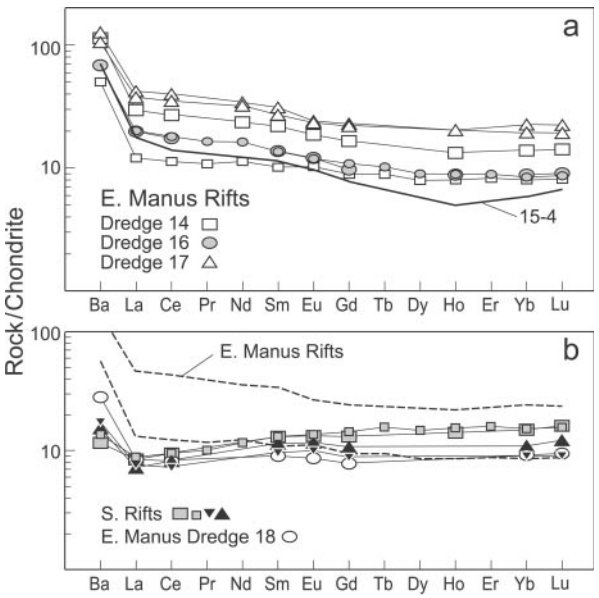

Fig. 8. Rare earth element and Ba concentrations for East Manus Rifts (a) and Southern Rifts (b) samples, normalized to C1 chondrite [values from Sun & McDonough (1989)]. Although SR samples have lower La/Sm than ER samples, both provinces have high Ba/La.

GEOCHEMICAL CHARACTERISTICS OF MANUS BASIN MAGMAS

Arc-like magmas

Lava samples from the ER include basalts and basaltic andesites with <55 wt % SiO_2, and andesites and dacites with >61 wt % SiO_2 (Tables 2 and 5). The basaltic andesites contain olivine, plagioclase and clinopyroxene, whereas the more silicic lavas contain plagioclase, augite, hypersthene and Fe-oxide. Arc lavas from the East Manus define compositional trends vs MgO with high SiO_2, Al_2O_3, alkalis, H_2O, Sr and Ba, and low TiO_2, FeO*, CaO, S, Sc, V, Cu, Zn, Y, Zr, Ni and Cr relative to Manus MORB. Low values of CaO, Sc, Zn, V, Cu and CaO/Al_2O_3 at high MgO in these lavas reflect the early fractionation of clinopyroxene, relative to Manus MORB. The low TiO_2, Y, Zr and Nb, high Sr, Ba, high Ba/La, presence of orthopyroxene, lack of Fe enrichment with progressive differentiation, and steady increase in SiO_2 with decreasing MgO are all characteristic of lavas associated with island arcs.

We recognize two types of arc lavas from the ER; those from dredge 14 (type A1) have distinctly lower K_2O, P_2O_5, Rb and Ba for a given MgO, slightly lower SiO_2, Na_2O, Y and Zr, and slightly higher FeO*, CaO, Sc, V and $Fe_2O_3/(FeO + Fe_2O_3)$ compared with those from dredges 15, 16 and 17 (type A2, Figs 4–6).

Lavas from the ER have $^{87}Sr/^{86}Sr$ >0·70355; all other samples in the Manus Basin have lower values, as do Quaternary lavas from eastern New Britain (Fig. 7). The REE patterns of analyzed ER lavas are also distinct from those elsewhere in the basin. Arc lavas from dredges 14–17 have similar, flat heavy REE (HREE; Gd to Lu), and slightly inclined LREE (Eu to La) patterns (Fig. 8). The REE patterns for both arc types A1 and A2 are similar. All ER lavas have Ba/La ratios >25.

MORB

Low K_2O, tholeiitic lavas were recovered from the MSC, ETZ and in dredge 23 from a seamount south of the SW end of the MSC (Fig. 2). On MgO variation diagrams, Manus MORB have the highest FeO*, TiO_2,

CaO, Zn, Y, Sc, V, Cu, Ni and Cr, and lowest K_2O, P_2O_5, Al_2O_3, Rb, Sr and Ba of any of the major magma types (excluding lavas from Group 31A) in the basin (Figs 4–6). Samples with MORB affinities range from high-Al basalt (RD 23, Table 5) through basalts and ferrobasalts with >17·5 wt % FeO* (total Fe as FeO) in dredge 46 (Tables 2 and 5), to dacites and rhyodacites with >66 wt % SiO_2. Manus MORB have the lowest H_2O and highest S contents, and are the least oxidized of any lavas from the Manus Basin (Fig. 6).

Petrographic inspection of the recovered samples indicates that Manus MORB with greater than ~8·5 wt % MgO are saturated only with olivine. Plagioclase joins olivine at bulk compositions less than ~8 wt % MgO, producing a decrease in CaO and Al_2O_3 with decreasing MgO. Manus MORB become saturated with clinopyroxene at 6·5–7·0 wt % MgO; the incoming of cpx results in a decrease in CaO/Al_2O_3, Sc and Cu, and inflections in the variation curves for Al_2O_3, V and Zn. These variations indicate that Sc, Cu, V and Zn are at least moderately compatible in MORB clinopyroxene from the Manus Basin. A reaction relationship between olivine and low-Ca pyroxene occurs near 4 wt % MgO, such that lavas with lower values of MgO contain pigeonite and no olivine. This reaction corresponds to inflections in the variation for Al_2O_3 and V (not shown). The sharp decrease in TiO_2, and FeO*, and associated increase in SiO_2 in lavas with less than ~2·5 wt % MgO corresponds to the incoming of oxide as a fractionating phase.

Even the most extreme differentiates of the MORB suite have <0·5 wt % K_2O at <1 wt % MgO, indicating that this suite is derived from primary magmas with extremely low K_2O values. This result contrasts with that for mid-ocean ridge silicic lavas; glasses from the East Pacific Rise with 64–66 wt % SiO_2 have 0·6–0·7 wt % K_2O (Sinton *et al.*, 1991), and those from the Galapagos Spreading Center near 95°W with ~66 wt % SiO_2 have nearly 1·3 wt % K_2O (Byerly *et al.*, 1976). Thus the Manus MORB suite is even more depleted in K_2O than are many Pacific MORB.

Manus MORB are strongly depleted in the LREE compared with HREE (Fig. 9). Although N-MORB from throughout the spreading ridge spectrum are depleted in LREE, Manus MORB are even more depleted in La, as well as K, Ta and Nb compared with average N-MORB (Fig. 10). These characteristics suggest that MORB from the Manus back-arc basin are even more depleted in some incompatible elements than are typical MORB, a result that also characterizes some arc and back-arc lavas in other areas (Woodhead *et al.*, 1993; Elliott *et al.*, 1997).

Manus MORB are slightly enriched in Cs, Rb, Ba, U, Pb and Li, relative to average N-MORB (Fig. 10). Enrichments in these elements are also characteristic of many arc and back-arc magmas. Thus, although MORB magmas from the Manus Basin can be considered to be the magma type least affected by subduction-related processes, coupled depletions in highly incompatible, high field strength elements (HFSE) and relative enrichments in the most incompatible lithophile elements are still apparent.

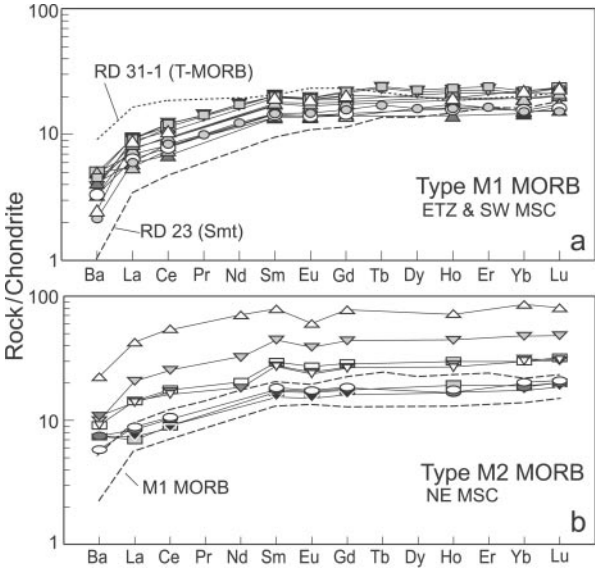

Fig. 9. Rare earth element and Ba concentrations for Manus MORB, normalized to C1 chondrite [values from Sun & McDonough (1989)]. All are depleted in LREE and Ba. Compared with M1 MORB, type M2 tend to have slightly higher La/Sm and Ba/La and range to more differentiated compositions. Negative Eu anomalies in the most differentiated samples with highest total REE indicate plagioclase fractionation.

We have separated the Manus MORB suite into two subtypes. Type M1 are MORB lavas from the ETZ and SW part of the MSC; in most characteristics these are normal MORB with the exception of those characteristics described above. High-MgO samples from the seamount (dredge 23) have been included with type M1, although they are more depleted in most incompatible elements than are other type M1 samples (see, e.g. Fig. 9). Type M2 lavas are from the NE part of the MSC; relative to M1, M2 MORB are more differentiated, and follow liquid lines of descent that project to parental magmas slightly enriched in K_2O and other LILE, and H_2O. Type M2 MORB tend to have higher Ba/La than M1 MORB (Fig. 9).

BABB

A suite of tholeiitic lavas plot subparallel to the MORB trend but are displaced to higher LILE, SiO_2, Al_2O_3, P_2O_5 and H_2O, and to lower FeO*, TiO_2, CaO and S contents

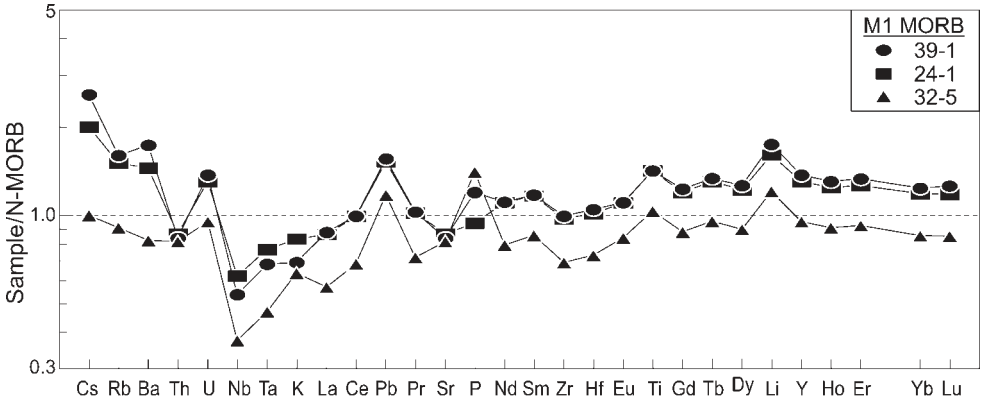

Fig. 10. Incompatible elements in Manus MORB glasses normalized to N-MORB [values from Sun & McDonough (1989)]. The relative enrichments in Cs, Rb, Ba, U, Pb and Li suggest that even Manus MORB have a contribution that can be related to dehydration of subducted slabs. Whether this contribution comes from present subduction beneath New Britain, or prior subduction beneath New Ireland (Woodhead *et al.*, 1998) is unknown.

at the same MgO (e.g. Figs 4–6). These are the characteristics of BABB from the Mariana Trough, Lau Basin, North Fiji Basin and East Scotia Sea (Saunders & Tarney, 1979; Fryer *et al.*, 1981; Sinton & Fryer, 1987; Johnson & Sinton, 1990). Manus BABB magmas appear to become saturated with clinopyroxene at higher MgO than for Manus MORB, as even the most primitive BABB rocks (MgO 9·3 wt %) contain euhedral clinopyroxene phenocrysts. Plagioclase joins olivine as a fractionating phase in Manus BABB at MgO contents of ~7·5 wt %, values slightly lower than for Manus MORB (~8·0 wt %). The delay in fractionation of plagioclase to lower MgO was ascribed to hydrous fractionation in Mariana Trough BABB (Sinton & Fryer, 1987). Measured H_2O contents are greater in Manus BABB than in Manus MORB at the same MgO (Fig. 6), suggesting that this interpretation also pertains to Manus BABB. The Manus BABB suite can be divided into three subtypes; ER BABB (Be, dredge 18), SR BABB (Bs) and those from the ETZ and MSC (B).

BABB lavas from the Manus Basin have REE patterns that vary from slightly LREE depleted to nearly flat (Fig. 11), similar to Mariana Trough BABB (Fryer *et al.*, 1981). Most BABB lavas from the MSC and ETZ have Ba/La ratios near 1·0, whereas those from the SR and ER have values >1·0 (Fig. 8). Manus BABB have similar $^{87}Sr/^{86}Sr$ to Manus MORB, but have lower $^{143}Nd/^{144}Nd$ and higher $^{206}Pb/^{204}Pb$, $^{207}Pb/^{204}Pb$ and $^{208}Pb/^{204}Pb$ (Fig. 7). In this respect, Manus BABB are isotopically similar to arc lavas from New Britain and the ER. Within the BABB suite, there is a range in the extent of enrichment in the elements characteristic of BABB (primarily H_2O, SiO_2, alkalis, Ba, Sr, LREE and Pb isotopes), relative to MORB. Thus, the BABB type can be viewed as having been derived by melting of sources variably enriched in BABB components.

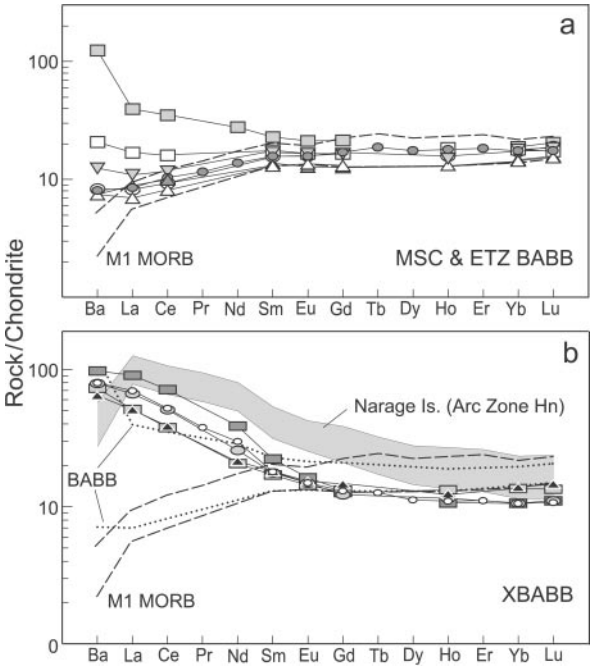

Fig. 11. Rare earth element and Ba concentrations for back-arc basin basalts from the Manus Spreading Center and Extensional Transform Zone (a) and for XBABB lavas from the Manus Spreading Center (b), normalized to C1 chondrite [values from Sun & McDonough (1989)]. It should be noted that sample 33-9 [shaded square in (a)] has moderately high La/Sm and Ba/La, similar to East Manus BABB (see Fig. 8). Shaded field in (b) encloses data for three samples from Narage in the northern Witu Islands [data from Woodhead *et al.* (1998)]. The BABB field from (a) is shown with a dotted line. The field of M1 MORB from Fig. 10 also is shown for reference.

XBABB

A suite of highly vesicular basaltic andesite and andesite lavas were recovered from the shallowest portion of the MSC. All contain microphenocrysts of plagioclase [typically An_{61-72} (Liu, 1989)] ± augite, olivine and/or orthopyroxene. Sample 35-3c is a glassy plagioclase + pyroxene-bearing gabbroic inclusion contained in sample 35-3. XBABB lavas plot within the arc field on many of

the variation diagrams against MgO (Figs 4–6). They can be distinguished from the arc lavas in having higher P_2O_5, Zr (Fig. 6), Nb and TiO_2. The Zr values are higher than those of MORB, whereas East Manus arc lavas have Zr contents less than those of MORB at the same MgO. XBABB have REE patterns that are distinctly different from those of Manus Basin arc lavas (compare Figs 8 and 11) and have much lower Ba/La ratios. The XBABB REE patterns are somewhat similar to those of lavas from Narage Is. (Witu Islands) (Fig. 11), although XBABB have higher La/Sm, flatter HREE patterns and much higher Ba/La.

Variations of several incompatible elements against MgO indicate that the variations within the XBABB suite cannot be explained by fractionation of a common parental magma. In particular, it is notable that the samples with the highest chondrite-normalized La have the lowest Yb. Such crossing REE patterns indicate evolution from a variety of parental magmas derived from mixing of at least two source components, one with high La, P and Sr, and low Yb. Those samples with the highest La/Sm also have the highest Sr (excluding cumulate sample 35-3c), and P_2O_5. We have divided Manus XBABBs into three subtypes (X1–X3), denoting parental magmas with progressively lower values of P_2O_5, Sr and La/Sm (Tables 2 and 5).

Group 31A

Group 31A lavas from the ETZ do not correspond to any of the above magma types. Compared with Manus MORB, they are slightly enriched in K_2O (Figs 3 and 4) and other alkali elements, similar to the BABB magma type. However, in contrast to BABB magmas, Group 31A also are enriched in many HFSE, especially TiO_2, P_2O_5 and Zr, and do not show characteristic BABB depletion in FeO*, or enrichment in Al_2O_3 and H_2O. Thus, Group 31A lavas tend to be enriched in all incompatible elements (except H_2O) relative to MORB, similar to lavas from oceanic islands and enriched MORB (E-MORB) from oceanic spreading centers. In general, ocean island basalts tend to have much greater incompatible element enrichments than do E-MORB (e.g. Sun & McDonough, 1989), which in turn are more enriched than some very mildly enriched transitional spreading center lavas (T-MORB). The modest incompatible element concentrations in Group 31A lavas are most like those of oceanic T-MORB.

REGIONAL VARIATIONS

Ocean island lavas

Volcanic rocks recovered from the vicinity of St. Andrew Strait on the Willaumez–Manus Rise (Johnson *et al.*, 1978; DePaolo & Johnson, 1979) have chemical affinities similar to some ocean island provinces, and the crustal structure of the rise (Johnson *et al.*, 1979) also is consistent with an hotspot origin. A fairly extensive lava flow field occurs in the southern part of our survey area bordering the Willaumez Rise (Martinez & Taylor, 1996; see also Fig. 1). Although this field was not sampled, we note that our dredge 31, which contained the only chemical group with enrichments similar to those occurring on oceanic islands, was taken from the southern part of the ETZ, proximal to the unsampled submarine Willaumez flows. Taken together, these data suggest that Quaternary volcanism with hotspot chemical affinities may be widespread on the Willaumez–Manus Rise.

Lavas from the Witu Islands (Johnson & Arculus, 1978) on the southern Willaumez Rise close to New Britain have diverse chemical characteristics. Aspects of their chemistry are similar to those of typical island arcs, consistent with their location over the deepest part of the New Britain Wadati–Benioff zone. Other chemical characteristics, such as enrichment in HFS incompatible elements, however, are similar to those of other lavas on the Willaumez Rise, and indicate affinity with ocean island (hotspot?) processes. The tectonic setting of the Witu Islands astride the Willaumez Rise behind the New Britain Trench is consistent with the complex chemistry of these lavas.

Macpherson *et al.* (1998) showed that high $^3He/^4He$ lavas occur all along the Manus Spreading Center and Extensional Transform Zone and argued for the presence of a deep mantle plume in the vicinity of the Manus Basin. These results are consistent with the presence of lavas with ocean island basalt affinities in St. Andrew Strait and on the Willaumez Rise (Witu Islands), although the exact center of any hypothesized plume remains unknown.

Low-K and medium-K arc lavas

Johnson (1976) divided the active arc of New Britain into two provinces: a western arc associated with the South Bismarck and Indo-Australian plates, and an eastern arc associated with subduction of the Solomon Sea plate beneath New Britain. Quaternary arc volcanism of the eastern arc is restricted to the northern shore and offshore islands of New Britain, and in the vicinity of Rabaul Caldera in NE New Britain. Johnson (1977) separated the eastern arc into zones that correspond to increasing depths to the Wadati–Benioff zone beneath New Britain (Fig. 12). Zones E and F comprise the volcanoes of the northern shore and nearshore islands, where the depth to the dipping seismic zone is less than $\sim$130 km. Zone G corresponds to volcanoes in the vicinity of the Willaumez Peninsula of New Britain, which are underlain

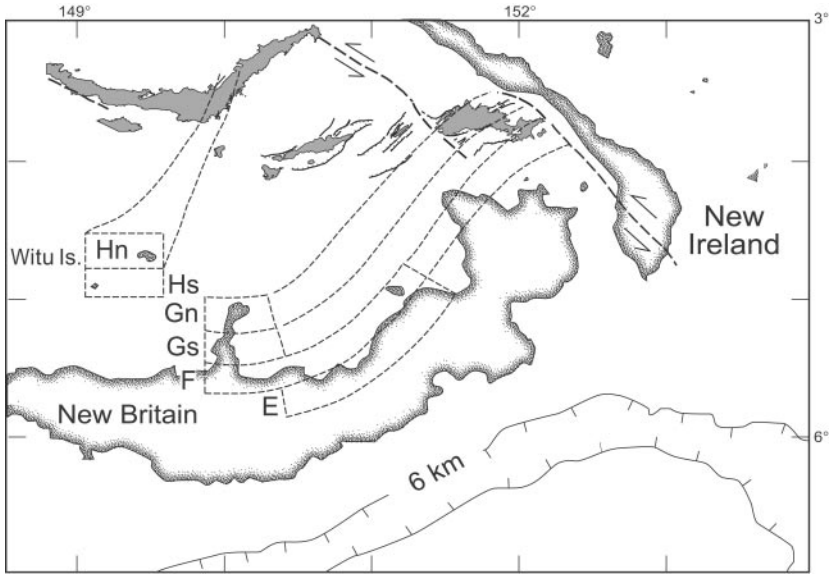

Fig. 12. Possible extension of the arc zones of Johnson (1977) to the submarine back-arc, based on geochemical data summarized in Table 7. The similarity between XBABB from the MSC and Witu Islands samples is discussed in a later section of the text.

Table 7: New Britain arc zones

Zone:	E	F	Gs	Gn	Hs	Hn	RD 14	RD 16–17	XBABB
Depth to WBZ (km):	~70–95	~95–130	~130–185	~185–295	~295–415	~415–540	~150–200	200–450	
Na_2O	2·51	2·49	2·35	2·90	3·21	3·45	~3·2	3·2	3·7
K_2O	0·43	0·50	1·01	0·91	1·29	0·67	~0·6	0·9	0·7
Sc	31	31	31	31	28	28	~33	32	26
Rb	5·9	6·2	11·1	10·7	19·5	9·6	~7	12	9·5
Zr	31	34	45	50	94	138	~39	55	120
Ba	92	110	179	185	143	90	~150	185	230
La	1·41	2·85	5·82	5·02	10·25	7·53	~4·5	5	21
Yb	1·23	1·53	1·44	2·11	2·31	3·84	~1·3	1·7	1·8
Hf	0·9	1·1	1·2	1·3	1·9	3·3	~0·7	1·2	2·1
$^{206}Pb/^{204}Pb$	18·72	18·75	18·72	18·69	18·65	18·50	18·80	18·74	18·74

Chemical characteristics of New Britain arc zones are normalized to $SiO_2 = 55$ (from Woodhead & Johnson, 1993). WBZ, Wadati–Benioff zone.

by a dipping seismic zone at depths between ~130 and 295 km. The Witu Islands lie above the deepest part of the Benioff zone (>295 km) and these volcanoes define zone H. Woodhead & Johnson (1993) showed that there are significant differences in average chemical and isotopic composition among these various zones (Table 7). For example, low-K arc volcanics occur in zones E and F, whereas zone G contains medium-K volcanic rocks.

Within the ER, both low-K (type A1) and medium-K (A2) rocks with arc affinity also are present. Samples from dredges 16 and 17 bear many similarities to those of Johnson's zone Gn (Table 7). Low-K samples from dredge 14 are most similar to Johnson's zone F, although the dredge samples have notably higher Na, La and Ba. Also, aspects of XBABB, recovered from the shallowest part of the MSC, are similar to some lavas from the northern Witu Islands (arc zone Hn). These include LREE-enriched patterns, along with high values of HFSE. These relations suggest that it may be possible to extend Johnson's zones to the submarine region as shown

in Fig. 12. As noted above, however, ER submarine lavas have higher $^{87}Sr/^{86}Sr$ than any analyzed New Britain arc rocks (Fig. 7). Although the New Britain volcanic arc zones were initially defined chemically, Woodhead & Johnson (1993) and Woodhead *et al.* (1998) showed that there also are systematic variations in Pb isotopes with slightly decreasing $^{206}Pb/^{204}Pb$ to the north. Although ER samples have relatively high $^{206}Pb/^{204}Pb$ compared with arc zones G and H, a general decrease in this ratio is apparent with distance when lavas from the MSC and ETZ are included (Woodhead *et al.*, 1998).

PETROGENESIS

Parental magma compositions and source heterogeneity

To assess variations in melting conditions and mantle sources contributing to Manus Basin magma compositions, it is necessary to correct for fractionation processes. Typically this is done by correcting data to a particular value of MgO or some other index of fractionation. For example, Klein & Langmuir (1987) used a constant slope correction for global MORB data to 8 wt % MgO, Plank & Langmuir (1988) corrected data from selected island arcs to 6 wt % MgO, and Woodhead & Johnson (1993) corrected New Britain arc data to 55 wt % SiO_2. For Manus Basin magmas a constant slope correction is inappropriate because most elements show variable slopes on MgO variation diagrams (e.g. Figs 4 and 5). Furthermore, because there is a change in slope when the fractionating sequence changes from olivine-only to olivine plus plagioclase, it is essential to carefully choose the reference value for corrections. For these reasons we have chosen the following procedure to deduce 'parental magma' compositions. For each magma type the MgO value where plagioclase joins olivine has been determined (Table 8). Petrography and relationships of CaO and Al_2O_3 vs MgO indicate that this value is $\sim$8·0 wt % MgO for Manus MORB. Experimental evidence shows that plagioclase joins olivine at progressively lower MgO values with increasing contents of H_2O (Yoder & Tilley, 1962; Nicholls & Ringwood, 1973; Bender *et al.*, 1978), and Manus magmas with progressively greater amounts of H_2O show a concomitant delay in the appearance of plagioclase (Table 8). All XBABB and type A1 samples have $\leq$6 wt % MgO, and all contain plagioclase, i.e. there are no olivine-only magmas. For these magmas the incoming of plagioclase is assumed to occur at the same MgO (7 wt %) as for type A2, because they have comparable H_2O contents. It should be noted that slight errors in this value will have little effect on the calculations that follow. Once the reference value (the minimum MgO for olivine-only magmas) has been identified for each magma type, slopes of oxides and elements on MgO variation diagrams have been determined by regression for all multiply-saturated samples (Table 8). With these slopes it is possible to correct all sample data back to the reference value.

Calculated parental magma compositions for selected elements are given in Table 9, and plotted against parental Y contents in Fig. 13. It is apparent that some HFSE are generally consistent with a model of progressive melting of a relatively depleted mantle source. For example, assuming that MORB type M1 magmas are generated by 10% partial melting, the sequence M2, B, Bs, Be, A2 follows trends of Nb, Zr and TiO_2 vs Y that are consistent with progressively increasing extents of partial melting of the same source. (Parameters used in the calculation of the melting model are given in Table 10.) It is notable, however, that >40% melting would be required to produce type A2 magmas, and even greater melting percentages for type A1. It also is obvious from Fig. 13 that XBABB must have formed from sources that had higher Nb/Y, Zr/Y and Ti/Y than the source for Manus MORB.

Although the HFSE are generally consistent with a common mantle source for some of the magmas in the Manus Basin, this scenario fails to account for the lithophile element variations shown in Fig. 13. Indeed, the incompatible elements Ba, K and Sr show progressive increases with declining parental Y through the sequence M1, M2, B, Bs, Be, A2, exactly the opposite of what would be predicted from progressive melting of the MORB source mantle. This result requires that mantle source heterogeneity plays a role in the genesis of Manus parental magma compositions. However, this heterogeneity is not random. The highest lithophile element concentrations occur in the magmas with the lowest Y contents. Through the sequence M1, M2, B, Bs, Be, A2, the increase in lithophile element concentrations with Y depletion shows a smooth trend, with a reversal to lower values of K and Ba for magma type A1 (Fig. 13). Thus, for the types M1–A2, lithophile element enrichment and Y depletion appear to be coupled. These data are summarized in Fig. 14, where it can be seen that, relative to M1, enrichments in Rb, Ba, K, Sr, and to a lesser extent La and Ce, are qualitatively tied to sympathetic depletions in Yb, Y, Ti, Zr, Sm and Nb. The relative depletions in Nb are critical because they indicate that the bulk partition coefficient during melting is not the controlling parameter, but rather chemical behavior that is probably related to slab dehydration processes (Tatsumi *et al.*, 1986). The order of enrichment is Rb > Ba > K > Sr > La > Ce $\geq$ P. Manus magmas are variably depleted in Sm, Zr, Ti, Y and Yb, with the exception of the XBABBs, which are enriched in P, Zr and Nb, relative to all other magma types. Thus, one hypothesis that would explain the coupled HFSE depletions with

Table 8: Parameters used for fractionation corrections

Type:	M1	M2	B	Bs	Be	A1	A2	X
Plag in:[1]	8·0	8·0	8·0	7·5	7·0	7·0	7·0	7·0
Slopes								
SiO_2	−0·53	−0·53	−1·01	−1·03	−1·13	−2·51	−2·35	−2·05
TiO_2	−0·30	−0·30	−0·15	−0·13	−0·10	−0·09	−0·09	(−0·09)
Al_2O_3	0·90	0·90	0·5	0·50	0·40	0·87	0·87	0·87
FeO*	−1·78	−1·78	−0·7	−0·7	−0·7	−1·40	−1·51	−0·77
CaO	1·05	1·05	1·05	1·05	1·05	1·39	1·39	1·20
Na_2O	−0·15	−0·15	−0·28	−0·27	−0·17	−0·36	−0·43	−0·17
K_2O	−0·004	−0·004	−0·07	−0·05	−0·04	−0·17	−0·17	(−0·17)
P_2O_5	−0·025	−0·025	−0·017	−0·017	−0·017	−0·035	−0·035	−0·018
Rb	(−0·4)	(−0·4)	(−0·4)	−0·22	−0·58	−2·30	−2·32	−2·04
Sr	1·67	1·67	−25·35	42·19	23·51	1·58	1·5	58·87
Y	−5·25	−5·25	−2·39	−3·50	−1·90	−2·54	−3·90	(−3·5)
Zr	−15·95	−15·95	−7·6	−10·6	−7·3	−11·80	−13·43	(−13)
Nb	−0·28	−0·28	−0·24	−0·25	−0·25	−0·35	−0·20	−0·30
Ba	−0·27	−0·27	−9·3	4·0	2·2	−44·08	−23·47	(−23)
La	−0·56	−0·56	−0·46	−0·46	−0·46	−1·42	−1·12	(−1·1)
Ce	−1·59	−1·59	−1·1	−1·1	−1·1	−3·28	−2·86	(−2·9)
Sm	−0·66	−0·66	−0·20	−0·2	−0·2	−0·61	−0·55	(−0·6)
Yb	−0·85	−0·85	−0·2	−0·2	−0·2	−0·34	−0·49	−(0·4)

[1]MgO (wt %) where olivine is joined by plagioclase in the fractionating assemblage. All oxide and element data are then corrected to this value using the slopes shown. For samples with MgO greater than this value, no fractionation correction is made.

LILE enrichments is for extent of melting (HFSE depletions) to be tied to fluid-related enrichments (LILE). In this case, the greatest slab flux would be to those magmas that were generated by the greatest extents of partial melting. Type A1 does not follow the coupled trends shown for the other MORB, BABB and A2 magma types, particularly with respect to K and Ba concentrations. This characteristic is a strong feature of the New Britain arc zone F relative to zone G (e.g. Johnson, 1977; Woodhead & Johnson, 1993) as discussed above.

Taken together, the results shown in Figs 13 and 14 suggest that a systematic set of processes can be invoked to explain the MORB, BABB and A2 magma types, but that some different processes have operated in the production of XBABB and A1 magmas.

Melting processes

In the presence of mantle heterogeneity, it is difficult to unambiguously constrain melting processes occurring beneath the Manus back-arc basin. However, some attributes of the parental magma compositions determined here are pertinent to procedures commonly employed in assessing mantle sources and melting processes. For example, Klein & Langmuir (1987) and Langmuir *et al.* (1992) showed that Na concentrations can be used to assess melting processes giving rise to normal MORB, with the implication that Na_2O is not widely variable in the sub-ridge mantle. Plank & Langmuir (1988) used a broadly similar approach to interpret aspects of melting beneath island arcs. However, whether or not Na is variable in mantle sources associated with subduction zones is an open question. The calculated compositions of hydrous fluids in variable equilibrium with Mariana Trough magmas are strongly enriched in Na (Stolper and Newman, 1994). Parental Na values for Manus magmas are shown in Fig. 15, where it can be seen that there is little variation in parental Na despite a wide variation in parental Y contents, in contrast to melting models which predict sympathetic decreases in Na and Y contents (Fig. 15a). One interpretation of this result is that Na has been enriched in mantle sources giving rise to BABB and arc magma types, i.e. that it has behaved similarly to other lithophile elements. If so, then its value as a monitor of melting extents cannot be used unambiguously in this setting. This interpretation does

Table 9: Parental magma compositions

Type:	M1	M2	B	Bs	Be	A2	A1	X1	X2	X3
SiO_2	50·3	50·7	50·2	50·7	51·9	51·3	49·0	51·2	51·2	51·3
TiO_2	0·97	0·86	0·76	0·71	0·47	0·39	0·47	0·57	0·67	0·71
Al_2O_3	14·8	15·1	15·6	15·9	16·4	17·1	18·0	18·3	17·8	17·8
FeO*	10·3	9·7	9·1	8·5	7·8	7·2	7·3	4·9	5·9	5·5
CaO	12·5	12·5	12·8	12·4	12·3	11·8	12·3	11·4	11·4	11·3
Na_2O	2·22	2·18	2·03	2·15	2·00	2·04	2·31	3·15	3·05	3·18
K_2O	0·05	0·06	0·07	0·20	0·29	0·64	0·19	0·33	0·29	0·10
P_2O_5	0·10	0·08	0·10	0·10	0·10	0·13	0·06	0·28	0·21	0·13
Rb	0·4	0·5	1·5	2·2	3·3	9·2	1·2	4·8	4·3	1·3
Sr	75	84	104	180	191	445	452	799	578	473
Y	24·5	23·3	18·8	16·1	10·8	7·9	7·5	6·9	9·8	7·9
Zr	51	46	42	37	27	25	12	90	71	54
Nb	0·9	0·9	0·6	0·6	0·5	0·4	0·3	5·2	4·3	3·0
Ba	9	15	13	33	66	148	49	182	137	92
La	1·39	1·15	1·57	1·58	1·98	3·39	1·02	18·95	13·86	8·57
Ce	4·72	3·84	4·89	4·46	4·96	7·23	1·38	36·77	25·45	14·09
Sm	2·15	1·76	2·09	1·63	1·37	1·41	0·28	2·01	1·49	0·78
Yb	2·55	2·08	2·57	1·87	1·55	0·82	0·64	0·87	0·97	1·06

not require that Y contents be uniform throughout the mantle beneath the Manus Basin, but only that Y is not mobilized during slab dehydration, an interpretation that is shared by most workers (e.g. McCulloch & Gamble, 1991; Woodhead *et al.*, 1993; You *et al.*, 1996).

Niu *et al.* (1996) used parental Ca/Al ratios to monitor total melting extents for a region where Na heterogeneity was suspected. However, the strong increase in parental Al with decreasing parental Y (Fig. 15b) produces a strong decrease in CaO/Al_2O_3 with decreasing Y contents because parental Ca does not vary much in Manus magmas (Table 9). The relationship of Ca/Al with Y is opposite to what would be expected from progressive melting of a common source. Hence, it is apparent that Ca/Al cannot be used unequivocally to assess melting extents and that Al also is likely to have been mobilized during slab dehydration processes in the Manus region, consistent with its high solubility in supercritical hydrous fluids (Schneider & Eggler, 1986).

Progressive melting vs prior depletion

In the above discussion, Y contents have been used as an index of the degree of depletion. Although residual garnet during melting can result in Y and HREE depletions, melting with residual garnet should produce inclined HREE patterns. Virtually all Manus Basin magmas have relatively flat, chondrite-normalized HREE patterns (Figs 8–11), indicating that garnet is unlikely to have been residual during melting events that produced them. In the absence of residual garnet, the relative depletions in Y, Yb, Zr and Nb in BABB and arc magmas, relative to MORB, can arise either from extremely high extents of melting of the MORB source, or from melting of sources that were already more depleted in Y and other HFSE relative to the source for MORB. This depletion could arise, for example, by previous melting events, possibly even before incorporation into the Manus back-arc setting. Thus, low Y contents might not signify high degrees of melting, but rather melting of a highly depleted source. Nevertheless, because BABB and especially arc magma types have higher water contents than Manus MORB (Fig. 6), relatively higher extents of melting giving rise to these magma types are to be expected as a result of solidus depression of hydrous mantle materials (e.g. Kushiro, 1968; Green, 1973; Stolper & Newman, 1994; Hirose & Kawamoto, 1995; Hirschmann *et al.*, 1998). Although higher melting extents giving rise to BABB and arc magma types might be expected, the quantitative model shown in Fig. 13 seems unrealistic, because melting extents >40–50% are required to match the Y contents of Manus arc types from sources similar to that giving rise to Manus MORB. Even in the presence of significant water contents, such extreme melting extents are unlikely, and exceed the expected increase in melting caused by addition of water alone (Hirose & Kawamoto,

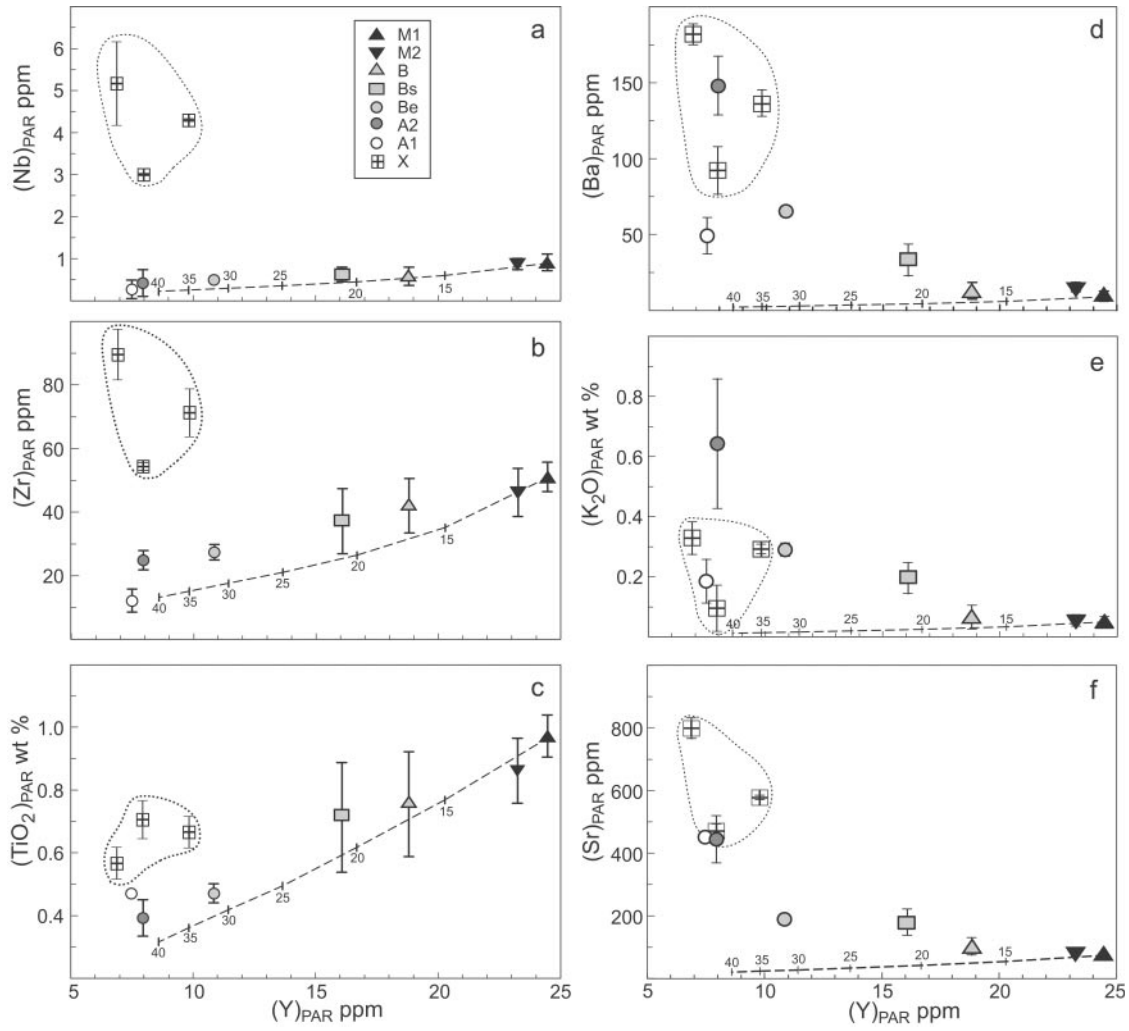

Fig. 13. Compositional variations for Manus Basin magmas types corrected for fractionation (PAR denotes parental composition, equivalent to the abundance at the MgO value where plagioclase joins olivine on the liquidus) vs parental Y contents. Vertical bars show ± 1 SD from the mean for each magma type. Also shown are the expected variations for a model of progressive melting (accumulated fractional melts) using the parameters given in Table 10. This model is set to produce MORB type M1 magmas at 10% total melting. Numbers next to the melting trend are in percent melt. Although the variations for Nb, Zr and Ti approximate a melting trend, those for Ba, K and Sr show progressive enrichments with decreasing parental Y contents. Magma types M1–M2–B–Bs–Be–A2 form coherent trends on these plots. A1 data plot off this trend for Ba and K. XBABB are enriched in Nb, Zr and Ti relative to the trends defined by the other data. (See text for discussion.)

1995; Hirschmann *et al.*, 1998). Hess (1992) showed that if fractional melting is operative then there are significant thermal barriers to melting above the exhaustion of major mantle phases, such as clinopyroxene or orthopyroxene. Clinopyroxene probably is removed at melting extents of the order of 18–22% (e.g. Langmuir *et al.*, 1992; Hirschmann *et al.*, 1998), and at 40–50% melting, orthopyroxene also might be exhausted, leaving only dunite residues with very high melting temperatures. There is considerable evidence that near-fractional fusion is common in upwelling mantle (Johnson *et al.*, 1990; Langmuir *et al.*, 1992). As such, melting percentages as high as those suggested by the model shown in Fig. 13 are unlikely.

Although BABB and arc magmas might have formed from higher melting extents than MORB, the strong depletions in Y and other HFSE suggest that they also formed from mantle that was already depleted by some prior event(s). Woodhead *et al.* (1993, 1998; see also Hochstaedter *et al.*, 2000) reviewed the arguments for high melting extents vs prior depletion, as well as the role of titanate phases, in producing Ti and other HFSE depletions in arc and back-arc magmas. Those workers strongly favored prior depletion in most arc and back-arc settings, and specifically argued for prior depletion in the history of New Britain arc magmas (Woodhead *et al.*, 1998). In any case, the relationships shown in Fig. 13 suggest that the greatest LILE enrichments to Manus

Table 10: Values used in fractional melting model

Modes F <0·22		Ol	Cpx	Opx	Sp
Start:		0·58	0·15	0·25	0·02
Melt:		0·10	0·68	0·20	0·02
Modes F >0·22					
Start:		0·25	0	0·73	0·02
Melt:		0·15	0	0·83	0·02
	C_0	K_d	K_d	K_d	K_d
Ti	761	0·016	0·3	0·1	0·1
Na	0·226	0·001	0·2	0·008	0·0001
K	41·7	0·001	0·0053	0·0039	0·0003
P	45·7	0·0002	0·2563	0·0145	0·0005
Sr	8·3	0·016	0·26	0·016	0·0001
Y	3·44	0·01	0·485	0·08	0·0078
Zr	5·3	0·01	0·1	0·05	0·05
Nb	0·09	0·002	0·005	0·0025	0·0004
Ba	0·9	0·001	0·001	0·001	0
La	0·139	0·0001	0·1	0·0053	0·0003
Ce	0·476	0·0001	0·1625	0·009	0·0005
Sm	0·244	0·0006	0·35	0·02	0·0009
Yb	0·403	0·03	0·4667	0·1	0·0045

F, fraction of melt; clinopyroxene is exhausted after 22% melting. Melt modes at F >0·22 are estimated from phase relations given by Hess (1992). C_0, composition of the starting material, before melting. These values are determined as those required to make parental M1 compositions at F = 0·10. The equation used is that for accumulated fractional melts (Shaw, 1970).

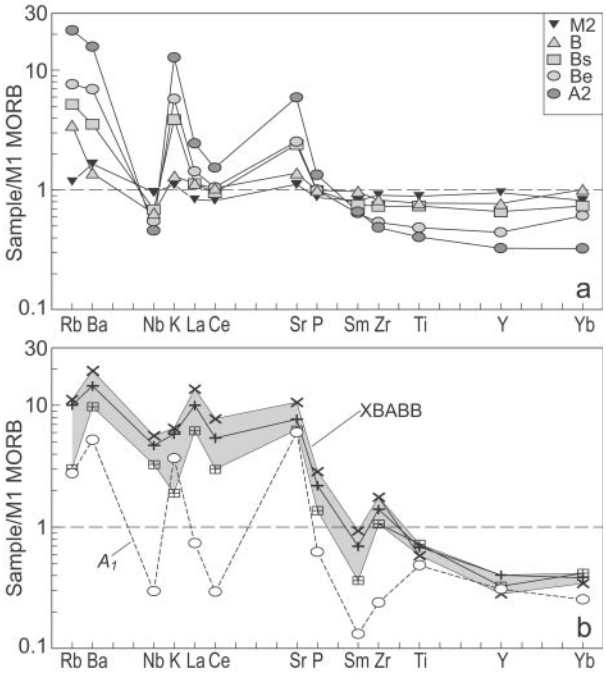

Fig. 14. Parental magma compositions normalized to values for parental magma type M1 MORB. (a) Magma types M2, B, Bs, Be and A2. (Note that all patterns cross between P and Sm.) (b) Parental magma compositions for type A1 (circles) and XBABB (shaded). (See text for discussion.)

back-arc magmas have occurred in those that are the most depleted in HFSE. This relationship is best explained by having slab flux to be greatest where the ambient mantle is most depleted. Such a situation could arise where there is a lateral variation in mantle depletion, with the most depleted mantle occurring closest to the arc volcanic front, a feature apparently common to many arc and back-arc systems (e.g. Woodhead *et al.*, 1993; Hochstaedter *et al.*, 2000; Martinez & Taylor, 2002).

The origin of lateral variations in mantle depletion can be explained as a natural consequence of prior melting processes coupled to mantle convection in the mantle wedge overlying subduction zones. Decompression melting accompanying mantle upwelling produces a vertical gradient in depletion of the residual melt column (Klein & Langmuir, 1987; Plank & Langmuir, 1992). Thus, where the ambient mantle composition is determined by prior melting, the residual mantle should be vertically zoned with the most depleted residual peridotites occurring in the shallowest mantle. As this vertically zoned mantle becomes incorporated into the advective regime of the mantle wedge overlying the subducted slab, depleted uppermost mantle should be dragged downward (Fig. 16). In this scenario, the shallowest mantle, and that closest to the volcanic front, will be the most depleted. Because the extent of slab dehydration should diminish with depth, the maximum slab flux should occur in the shallowest regions adjacent to the downgoing slab. Therefore both mantle depletion and slab flux will be maximized in the shallowest mantle close to the subducted slab. Although convective overturn might allow depleted mantle to exist over a considerable range of depths close to the slab, the shallowest mantle should still be the most depleted. Farther out into the back-arc basin mantle depletion will vary more regularly with depth.

Depths of melt generation

There are fewer unambiguous geochemical constraints on the depth of magma generation than for melting extents. However, a large body of isobaric experimental evidence indicates that silica decreases and iron increases with depth of melting (e.g. Jaques & Green, 1980; Falloon *et al.*, 1988; Falloon & Danyushevsky, 2000). In the case of polybaric, decompression melting associated with mantle upwelling, iron and silica contents have been

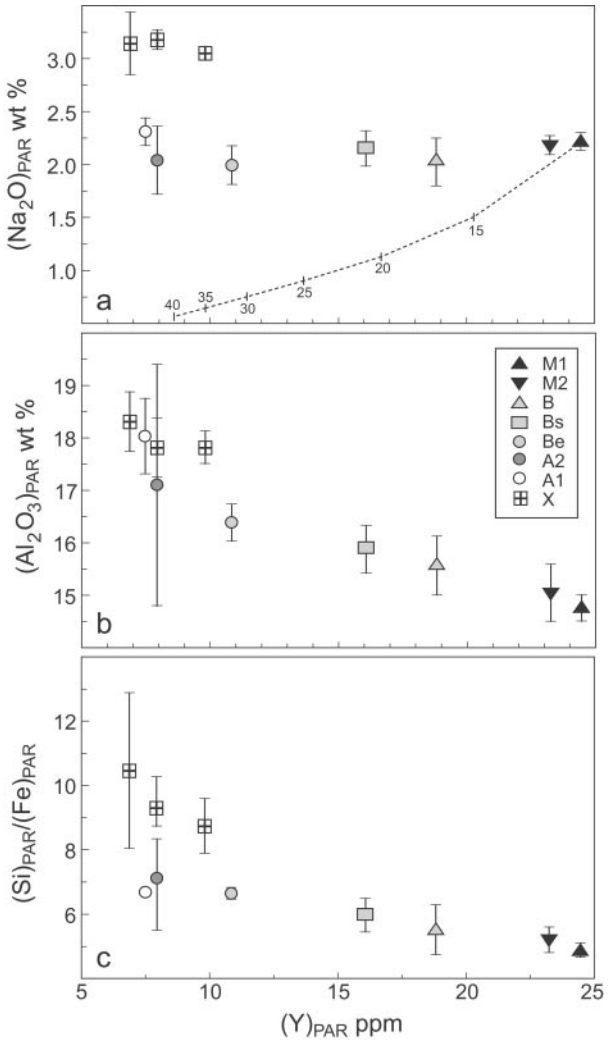

Fig. 15. Na_2O, Al_2O_3 and Si/Fe (SiO_2/FeO*) for parental magma compositions plotted against parental Y contents as in Fig. 13. All symbols and the melting model are the same as in Fig. 13. The variations for Na and Al suggest that these elements may be involved in mantle metasomatic processes, similar to arguments for other LILE. Si/Fe is commonly taken as an inverse index of melting depth (e.g. Niu & Batiza, 1991, 1993), but also can be affected by hydrous melting, especially at low pressure (Falloon & Danyushevsky, 2000).

used to constrain the depths of solidus intersection (e.g. Klein & Langmuir, 1987; Niu & Batiza, 1991; Langmuir *et al.*, 1992). Niu & Batiza (1991, 1993) used Si/Fe, corrected for fractionation, as an inverse index of the pressure of melting (Si/Fe decreases with depth of solidus intersection). Si/Fe of parental magmas of the Manus Basin systematically increase with decreasing parental Y contents (Fig. 15c). If this ratio is controlled by melting depth in these back-arc basin lavas, then it argues for progressively shallower melting through the sequence MORB–BABB–A2. XBABB have the highest Si/Fe and, according to the same reasoning, represent the shallowest melts in the basin.

The above reasoning primarily pertains to anhydrous melting. However, in subduction-zone settings there are two additional processes that can potentially affect magmatic silica concentrations. Nakamura & Kushiro (1974) demonstrated high solubility of SiO_2 in supercritical aqueous fluids in equilibrium with mantle assemblages, indicating that SiO_2 might be a significant component of slab-derived fluids. Thus, one might expect those magmas most enriched in slab-derived components to show silica enrichment irrespective of their depths of melt generation. If mantle melts mix with SiO_2-rich fluids derived from the subducted slab then these mixed melts might show anomalously high Si/Fe. In a later section we present arguments that the slab-derived component beneath the Manus Basin is primarily present in solid, hydrous phases formed by open-system metasomatic processes in the mantle wedge and that there is no compelling evidence for a free fluid phase in the generation of Manus Basin magmas. The silica content of mantle melts is primarily controlled by pseudo-invariant relations in simple models of peridotite melting, and not by the silica content of the mantle assemblage (e.g. Hess, 1992). Thus, in the absence of a free fluid phase in the source region of Manus Basin magmas, the likelihood of slab-derived silica enrichment is greatly diminished.

It has long been recognized that the formation of quartz tholeiites, which are common in arc environments, is favored by melting at low pressure (e.g. Green, 1971). However, the addition of water to peridotite sources greatly expands the olivine volume and leads to the production of quartz tholeiites over an expanded depth range (Nicholls & Ringwood, 1973). According to Green (1973), the depth range over which silica-rich magmas can be produced increases with water content. Melting experiments of Falloon & Danyushevsky (2000) on depleted mantle assemblages at appropriate pressures and water contents show that maximum Si/Fe is produced from hydrous (H_2O-undersaturated) melting at 1·5 GPa (Fig. 17). At 2·0 GPa, addition of water markedly depresses the cotectic to lower temperature, but there is little change in SiO_2, FeO or Si/Fe of the resultant melts (Fig. 17). These data indicate that hydrous melting can increase the Si/Fe of mantle melts at low pressure, but this effect is greatly reduced at higher pressures. Magmas with Si/Fe >6·5, comparable with those of Manus Basin magma types Bs, A1 and A2 (Fig. 15) were only produced at 1·5 GPa under H_2O-undersaturated conditions (Fig. 17).

The above discussion suggests that the increasing Si/Fe through the sequence MORB–BABB–A2 is favored by a decrease in the depth of melting, and/or an increase in the water content of the mantle assemblage. Si/Fe of magma types Bs, A1 and A2 probably require a combination of low melting pressures and hydrous source

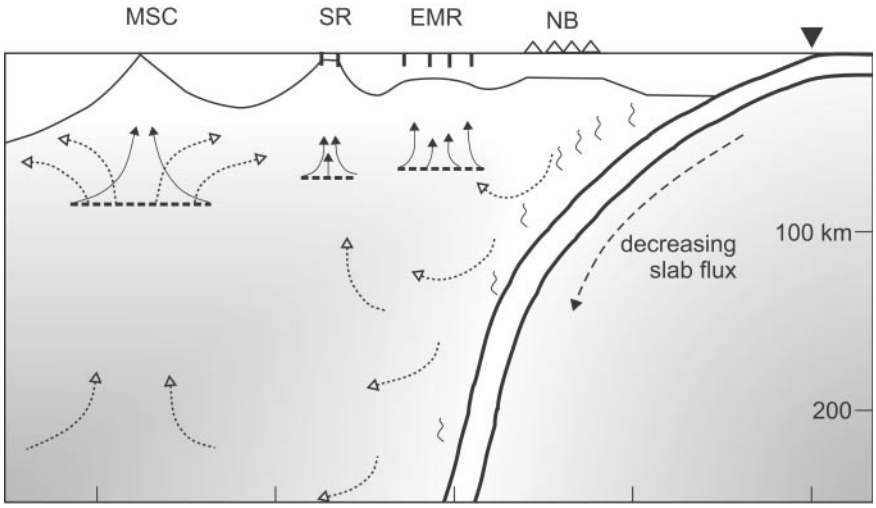

Fig. 16. Cross-section in the Manus Basin region showing melting processes occurring in the back-arc basin. MSC, Manus Spreading Center; SR, Southern Rifts; EMR, East Manus Ridges; NB, New Britain arc volcanoes. Location of the axis of the New Britain trench is shown by the solid, inverted triangle. The dip along the subduction zone is taken from Cooper & Taylor (1989). Hypothetical mantle flow trajectories are shown as short-dash lines; melt flow trajectories as continuous lines. Schematic relative melt depletion in the mantle is shown by a gradient in shading, with heavy shading being less depleted. It should be noted that SR and EMR zones could be sampling mantle that was previously depleted by melting at the Manus Spreading Center. This scenario is not required, however, because any model for previous melting should produce a vertical gradient in melt depletion, whether from nearby, recent melting, or ancient melting from unknown provinces (see text). Bold dashed lines denote the approximate positions of the solidi beneath the MSC, SR and EMR, consistent with Si–Fe relations shown in Fig. 15, and as discussed in the text.

peridotites. This result is somewhat counter-intuitive because of the well-known depression of peridotite solidi with increasing water contents (Kushiro, 1968; Green, 1973; Stolper & Newman, 1994; Hirose & Kawamoto, 1995; Hirschmann *et al.*, 1998; Falloon & Danyushevsky, 2000). Upwelling hydrous peridotites would be expected to cross their solidi at greater depth and experience more melting than upwelling anhydrous peridotite with the same potential temperature. However, the upwelling of hydrous peridotite probably is not the process that controls melting depth in the Manus Basin. Rather, close to the subducted slab, melting probably is initiated by the addition of water to ambient mantle peridotite. When the initiation of melting is controlled by the 'flux melting' process, rather than simply by decompression, melting depth may be controlled more by the position in the back-arc where water is being added than by the depth of the solidus of hydrous peridotite. Geometrical considerations for the New Britain–Manus Basin region effectively preclude deep hydrous melting beneath the New Britain arc volcanoes (Fig. 16), indicating that shallow hydrous melting may be a common process in this region.

A self-consistent model for the sequence MORB–BABB–arc basalt

As demonstrated above, the sequence from MORB to arc basalts forms strongly coherent trends on plots of various chemical parameters for the parental magmas vs parental Y. These include HFSE depletions nearly coincident with progressive melting of a MORB mantle, strongly coupled to increasing LILE and Al enrichments that presumably derive from increasing additions of dehydration products from subducted slabs. In addition, the varying Si/Fe are consistent with progressively shallower melting through this sequence. Relative to type M1, succeeding magma types in the sequence probably formed by progressively greater extents of melting, at least in part triggered by influx of slab-derived components at progressively shallower melting depths. These relationships are incorporated into Fig. 16. It is notable that much of the 'prior depletion' required to explain the HFSE depletion in BABB and arc magmas could have resulted from melting occurring at the Manus spreading center, although more ancient melt-depletion events are also permitted.

A fully quantitative model for melting processes giving rise to Manus back-arc magmas requires incorporation of a systematic ambient mantle depletion with depth of melt generation, coupled to a systematic depth-dependent variation in slab-derived components. However, there are too many uncertainties in this model to make it a worthwhile undertaking at present. One source of uncertainty is the nature of the slab-derived component, i.e. whether it is fluid, or metasomatized mantle, or melts derived from various components of the slab. Although this question is explored below, the greatest uncertainty

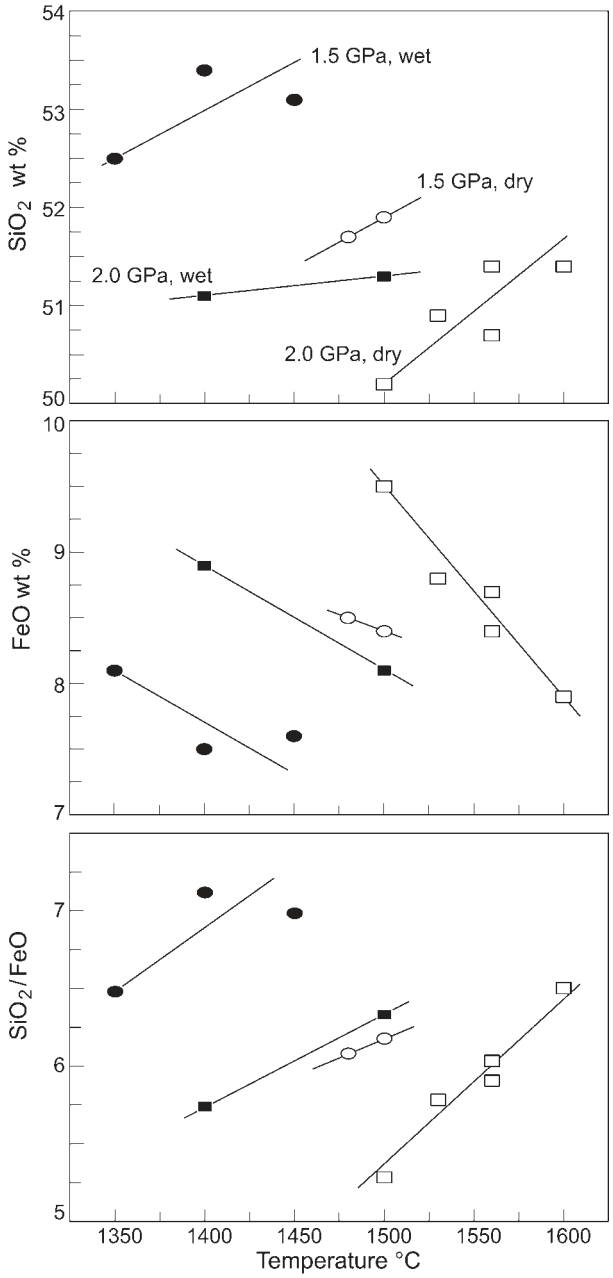

Fig. 17. Compositions of ol + opx-saturated liquids from anhydrous ('dry'; open symbols) and H_2O-undersaturated ('wet'; filled symbols) harzburgite reaction experiments at 1·5 GPa (circles) and 2·0 (squares) GPa, using data of Falloon & Danyushevsky (2000). Addition of water produces a pronounced decrease in the ol + opx + liquid cotectic temperature at both pressures. Addition of H_2O at 2·0 GPa produces little change in SiO_2/FeO. Liquids with SiO_2/FeO >6·5, comparable with those of Manus Basin magma types Bs, A1 and A2 (Fig. 15) were only produced at 1·5 GPa under H_2O-undersaturated conditions.

precluding a fully quantitative model derives from inadequate knowledge of the melting relations and partition coefficients pertaining to the melting of hydrous and/or metasomatized peridotites containing hydrous phases.

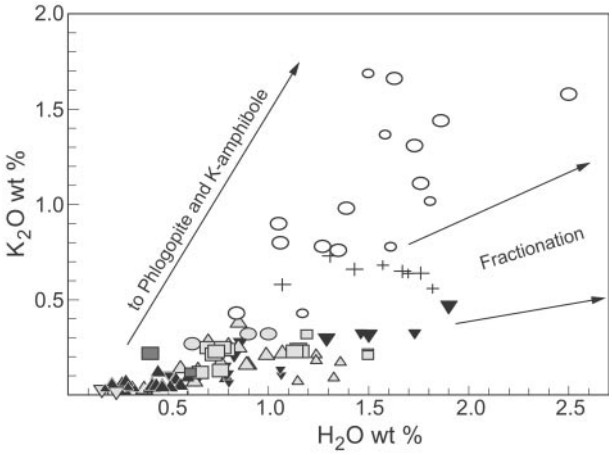

Fig. 18. K_2O vs H_2O in Manus Basin magmas (symbols as in Fig. 4). Magmatic fractionation within magma types produces a strong increase in H_2O with a modest increase in K_2O. In contrast, the variation between magma types requires addition of a component with K_2O/H_2O ~2. Both phlogopite and K-amphibole meet this requirement. Such phases would be produced by reaction between ambient mantle and hydrous fluids derived by slab dehydration (e.g. Sekine & Wyllie, 1982). We propose that hybridized solid mantle containing a K-rich hydrous phase becomes incorporated into the mantle flow regime in the back-arc basin, as shown schematically in Fig. 16.

Nevertheless, the qualitative scenario for progressively shallower melting of originally more depleted mantle that has been progressively enriched in slab-derived components as the trench axis is approached from the back-arc side is consistent with the available evidence.

The nature of the slab-derived component(s)

The variation of K_2O with H_2O in submarine Manus magmas is shown in Fig. 18. Two processes can be invoked to explain the spread of data on this diagram. Within magma types, fairly shallow sloping variation reflects fractionation processes; fractionation of Manus arc magmas produces a somewhat steeper trend [(K_2O/H_2O) ~0·5] than does fractionation of Manus MORB [(K_2O/H_2O) ~0·25]. These two values of K_2O/H_2O bound the variation owing to fractionation in Manus magmas; the slopes represent the ratios of the bulk partition coefficients for K_2O and H_2O during fractionation. Thus, fractionation can explain much of the variation in H_2O on this diagram, but only about a quarter to a half of the range in K_2O. Therefore another process must be invoked to relate the variation in K_2O and H_2O in magmas parental to Manus Basin lavas. The array of parental magmas in this plot lies to the left (low-H_2O) side of the data array, especially considering that most of the arc-type magmas are significantly differentiated. Thus, the relative enrichments in K_2O and

H_2O in parental magmas, i.e. between magma types, is of the order of 2:1. Because this enrichment appears to be a characteristic of the parental magmas, it must arise from melting, either because of variations in the melting process or from source compositional variations.

In the presence of mantle source variations, the relative partition coefficients cannot be calculated unambiguously from chemical variations alone. The simplest explanation for the relationships shown in Fig. 18 is that the K-rich arc magmas formed from sources with K_2O/H_2O much higher than that for MORB. Because we have argued above that extents of melting probably were at least as high for arc magmas as for MORB, then it is unlikely that the relationships in Fig. 18 are produced by residual K-rich phases. If so, then the slab-derived component that relates the BABB and arc magmas to MORB must have K_2O/H_2O ratios close to 2:1. A number of solid phases fit this requirement, most notably phlogopite and various potassic amphiboles. In contrast, the K_2O/H_2O ratios of fluids formed during slab dehydration are very low; Tatsumi & Kogiso (1997) inferred values of 0·05–0·17. Thus, the slab-derived component responsible for relating BABB and arc magma types to MORB in the Manus Basin is most likely to be in solid phases rather than fluids. Fluids derived from the breakdown of hydrous phases in the downgoing slab will react with the overlying mantle wedge in a process akin to open-system metasomatism (e.g. Sekine & Wyllie, 1982; Wyllie & Sekine, 1982; Sudo & Tatsumi, 1990). As K-bearing, hydrous fluids pass through the mantle, potassium and H_2O will be extracted from the fluid and fixed in the hybridized peridotites in the proportions dictated by the reactants, i.e. amphiboles and/or micas. Excess fluid, relatively depleted in K by these reactions, can continue to migrate through the convective regime of the mantle wedge. Evidence presented in this paper and many others indicates that other elements in addition to K and H_2O, most notably Rb, Ba, U, Pb, Sr, La and Ce, also become fixed in the modified mantle peridotite.

Once the K_2O/H_2O of the modified mantle has been fixed in solid phases, the subduction-related component can migrate within the back-arc convective regime. This is one explanation for how magmas showing the imprint of a slab component can be found in eruptive centers that do not overlie even the deepest portion of the subducted slab. This is the case for the Manus spreading center as well as for BABB lavas of the East Scotia Sea. It is worth emphasizing that the element concentrations in back-arc magmas reflect the combined pathway from possibly multiple episodes of slab dehydration and mantle metasomatism, as well as eventual melting giving rise to the recovered magmas. In light of this situation, it is perhaps surprising that most of the Manus magmas show relatively coherent and systematic trends. This result suggests that the composition of the solid, subduction-related component is relatively uniform in many chemical characteristics, as would be expected if composition is controlled by solid-phase stoichiometry and partitioning rather than fluid composition.

East Manus magmatism

The model for progressive metasomatism of progressively depleted mantle should produce a decrease in Zr/Y with increasing Ba/La, as shown by the higher Ba/La and low Zr/Y of subaerial arc magmas of zones E and F, relative to Manus MORB (Fig. 19). However, two groups of magmas have Zr/Y values higher than predicted by this general model. Specifically, arc zone H lavas have moderately high Zr/Y at low Ba/La (Fig. 19), and XBABB share this characteristic with even higher Zr/Y >10. These lavas are discussed in the following section. Also notable for relatively high Zr/Y at moderate Ba/La are submarine back-arc lavas from the ER. The chemical characteristics of East Manus lavas deviate from the general model outlined in previous sections, indicating some additional complications affecting magma compositions in this region.

Although ER magmas are generally similar to those of arc zones F and G (Table 7, Fig. 12) there are some notable differences. ER lavas have $^{87}Sr/^{86}Sr$ higher than any others from the region, including those of the subaerial New Britain arc volcanoes (Fig. 7). Other characteristics of ER magmas, compared with arc zones F and G, include moderately high $^{206}Pb/^{204}Pb$, exceptionally high Na_2O (Table 7), and Zr/Y values even higher than for Manus MORB (Fig. 19). The high Zr/Y of ER magmas can be deduced from Fig. 5, where it is apparent that ER magmas have much less Y with only slightly lower Zr at a given MgO compared with MORB. This is evidence that Zr and Y concentrations are somehow decoupled from the general melt depletion scenario outlined in previous sections.

If one considers the high Zr/Y of ER magmas to reflect relatively undepleted mantle, then their position in Fig. 19 suggests unusually high contribution from slab components (high Ba/La) to relatively undepleted mantle. However, this scenario is not in agreement with the unusually low Y, or most other HFSE contents of ER magmas (Figs 5 and 13); melting of less depleted mantle should produce magmas with higher Y and Zr, albeit with slightly higher Zr/Y. Thus the overall compositions of ER magmas do not indicate less overall incompatible element depletion, but rather extreme depletion in Y and Yb (Fig. 14) with less depletion in Zr. Thus the explanation for high Zr/Y, Na and $^{87}Sr/^{86}Sr$ cannot be ascribed to relatively undepleted mantle sources in this region. The unusual characteristics also are unlikely to

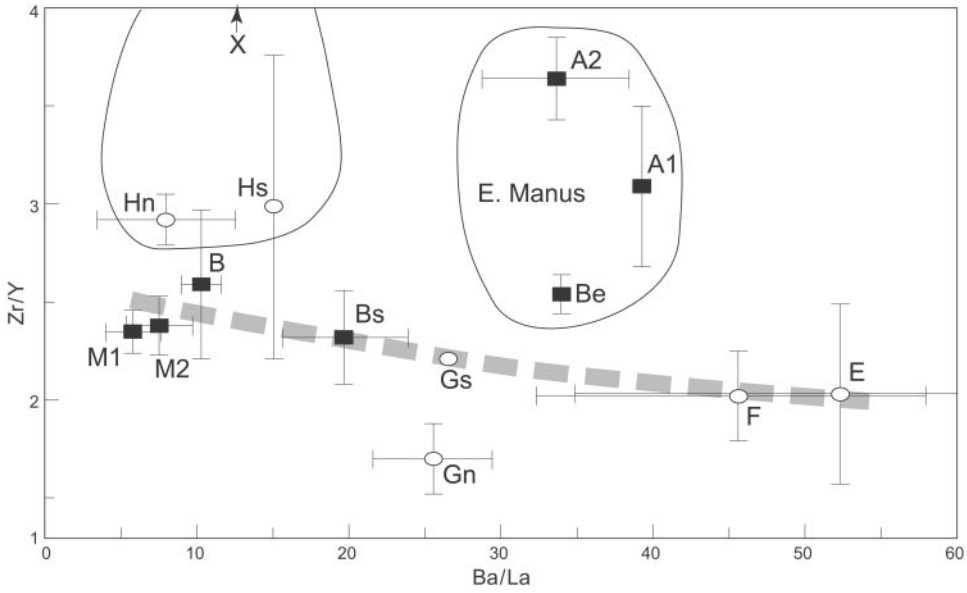

Fig. 19. Zr/Y vs Ba/La for samples from the Manus Basin–New Britain region. Data are shown only for samples with <55 wt % SiO_2. Data for New Britain arc samples are from Woodhead *et al.* (1998). There is an increase in Ba/La through the sequence Manus MORB–BABB–submarine arc to New Britain arc, which generally represents decreasing distance from the New Britain trench. Subaerial arc samples from zones E and F have lower Zr/Y than any of the submarine back-arc samples, consistent with their formation from more melt-depleted mantle. The trend of decreasing Zr/Y with increasing Ba/La is consistent with a model for progressive addition of subduction-related components to increasingly depleted mantle. According to this scenario the source for arc zone Gn magmas was unusually depleted. Two sample suites have unexpectedly high Zr/Y for their Ba/La. Samples from the Witu Islands (zones Hn and Hs) and XBABB have high Zr/Y at relatively low Ba/La. We interpret these magmas to have been affected by carbonatite melts in their source region (see text). Lavas from the ER (magma types Be, A1 and A2) have high Zr/Y at moderate Ba/La. In these magmas, Zr enrichment is accompanied by increases in Na (Table 7) and $^{87}Sr/^{86}Sr$ (Fig. 7), possibly as a consequence of crustal interaction in a zone of incipient rifting. (See text for discussion.)

be produced by lower extents of partial melting (as might be supposed from the high Na contents), because this would produce enrichment in both Y and Zr, and not produce the anomalous Sr and Pb isotopic ratios. This suggestion also is not in agreement with the high H_2O contents of ER magmas, which should correspond to relatively high extents of melting. Thus, explanations involving less depleted mantle and lower extents of melting of otherwise normal (for the Manus back-arc region) mantle fail to explain the combination of compositional characteristics observed. The failure of melting explanations for ER magma compositions leads us to consider processes that would allow enrichment of ER magmas with a component high in Zr, Na and $^{87}Sr/^{86}Sr$.

In contrast to the other back-arc zones in the Manus Basin, the ER show very limited, local zones of positive magnetization, suggesting that this is a zone of crustal stretching and incipient rifting (Martinez & Taylor, 1996). Little is known about the nature of crust in the eastern Manus Basin, although Martinez & Taylor (1996) suggested that it is of island arc origin, presumably formed in the Tertiary, associated with southwestward subduction along the now inactive Manus Trench (Fig. 1). Given the nature of the setting of the ER, it is worth considering crustal interaction as a possible explanation for the unusual compositions of lavas erupted there. Macpherson *et al.* (1998) found evidence for contamination of ER magmas with radiogenic He ($^3He/^4He$ <1) and Shaw *et al.* (2001) found air-like Ne isotopic compositions in ER magmas, both characteristics consistent with crustal interaction. However, it is notable that Macpherson *et al.* (2000) reported uniformly high $\delta^{18}O$ values for East Manus lavas, similar to mantle values. Thus, if crustal interaction is responsible for the low He and Ne isotopic compositions as well as the Zr, Na and ^{87}Sr enrichments, then this interaction has occurred without affecting oxygen isotopes. Because the Manus Basin is at low latitude (Fig. 1), the effect of meteoric water contamination on $\delta^{18}O$ will be much less than at higher latitudes. Furthermore, if ER magmas assimilated lower-crustal materials that had not been significantly altered, then no oxygen isotope signal would be expected. In summary, there is supporting evidence for crustal interaction (assimilation?) in the easternmost Manus Basin, and it is at least plausible that this interaction could lead to increased Na, Zr and $^{87}Sr/^{86}Sr$. The lack of well-organized seafloor spreading in this zone, and the generally differentiated nature of the magmas erupted there are consistent with a scenario for long-term storage and interaction with crust beneath the ER.

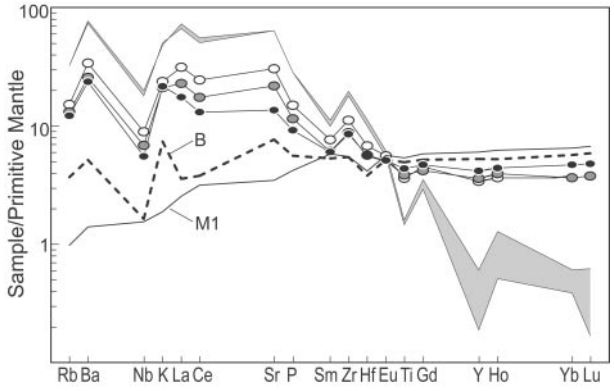

Fig. 20. Primitive mantle-normalized variations for XBABB, MORB type M1 and BABB. Shaded region shows the compositional range of a component required to mix with either MORB (M1) or BABB (B) to produce XBABB type X1 (unfilled circle). A mixing process for XBABB is consistent with the crossing REE patterns shown in Fig. 11. Model component compositions were derived by assuming that parental magma type X1 is a product of mixing of the unknown component with either parental MORB or BABB. The requirement that the abundance of all elements must be positive greatly restricts the proportions of the mixing end-members. Results shown here are for a MORB fraction of 0·55 and a BABB fraction of 0·60. Using the derived component composition restricts the component proportion range to 0·45–0·26 assuming mixing is with MORB or 0·40–0·18 if the component mixes with BABB. Although a unique solution to the mixing equations cannot be determined, this exercise demonstrates that the component composition must be strongly enriched in LREE, Sr, P and Zr, and strongly depleted in HREE. Although any garnet-dominated residue could produce HREE depletion and crossing REE patterns, the associated enrichments in Sr, P and Zr are especially consistent with carbonatite melts. It is notable that the model component also must have negative, mantle-normalized anomalies for Y, Ti and Nb, characteristic features of island arc lavas that are commonly ascribed to subduction-related metasomatism. (See text for discussion.)

Origin of XBABB and arc zone H

Although XBABB share many chemical characteristics with the arc-type lavas of the Manus Basin (e.g. Figs 3–6), they can be distinguished from the Manus arc lavas in having higher P_2O_5, Zr, Nb and TiO_2, and strongly LREE enriched patterns (Fig. 11). As noted previously, XBABB cannot all be related to fractionation from a common parent, but rather require derivation from a range of parental magmas produced by mixing of at least two source components, one of which has high La, P and Sr, and low Yb. XBABB have only been found on the MSC where the other rock types present are MORB type M1 and BABB. To assess the nature of mantle components contributing to XBABB, a series of mixing calculations have been performed using average M1 MORB and MSC BABB compositions. The compositional range of the required XBABB component is shown in Fig. 20. A notable characteristic of this component is enrichment in P along with LREE relative to Ti, similar to peridotites from Victoria, Australia, that Yaxley *et al.* (1991) interpreted to have been modified by interaction with carbonatitic melts.

Green & Wallace (1988) and Wallace & Green (1988) showed that sodic, dolomitic carbonatite melts can coexist with pargasite-bearing peridotite in a distinctive P–T–f_{O_2} window that is applicable to the mantle wedge overlying subduction zones. At P <2 GPa, and f_{O_2} greater than the enstatite + magnesite + olivine + graphite buffer, infiltration of carbonatitic melts into pargasitic peridotite results in reaction to form apatite-bearing wehrlite with enrichments in LILE and phosphorus. The role of the carbonatite melt is particularly effective at fractionating P and LILE from HFSE such as Ti and Nb, and can result in high P_2O_5 abundances and moderate to extreme LILE enrichment that is decoupled from Ti abundances (Wallace & Green, 1988). Enrichment in P and relative depletions in Nb, Ti and Y are characteristics of the XBABB component shown in Fig. 20. The chemical signature of this process has now been recognized in a number of xenoliths from intraplate environments (e.g. Yaxley *et al.*, 1991; Hauri *et al.*, 1993; Sweeney, 1994). Despite the arguments of Green & Wallace (1988) and Sweeney (1994) that conditions in the mantle wedge overlying subduction zones could be ideal for the coexistence of carbonatite melt with pargasite- or phlogopite-bearing peridotite, this process has not previously been identified in arc or back-arc environments.

The overall chemical signature of XBABB, as well as lavas from arc zone H, includes enrichments in Rb, Ba, Sr and Zr, in addition to P and the LREE. Some of these characteristics may derive from slab-derived components, similar to the case for BABB and arc magmas in the basin. However, chemical data for XBABB, as well as samples from the Witu Islands, are also consistent with a mantle that has been modified by both slab-derived fluid metasomatism and carbonatite melts.

CONCLUSIONS

The range of magma types in the Manus Basin can be related to generally systematic variations in mantle partial melting, prior depletion, and addition of subduction-related components. This principal subduction-related component probably takes the form of phlogopite-and/or K-amphibole-bearing peridotite that formed by reaction with fluids derived from dehydration of the subducted slab in the New Britain subduction zone. Manus MORB show the lowest melting extents of mantle that is the least depleted by prior melting, and experienced the least contribution from subduction-related components. There are coupled, systematic increases in melting extent, amount of prior depletion and amount of metasomatic enrichment through the sequence M1–M2–B–Bs–Be–A2–A1, which generally represents decreasing distance to the New Britain island arc. When compared with

chemical variations within subaerial New Britain arc volcanoes, magmas from the ER deviate from the general model in being unusually enriched in Na, Zr and $^{87}Sr/^{86}Sr$, possibly indicating crustal interaction in the zone of incipient rifting of ancient arc crust between the Weitin and Djaul transforms. In addition to the component produced by interaction of ambient mantle with subduction-related fluids, XBABB magmas require a component that is strongly enriched in LREE, P and Zr, similar to carbonatite melts, previously predicted to occur in subduction-zone environments.

ACKNOWLEDGEMENTS

The Captain and crew of R.V. *Moana Wave* cruises MW8517 and 8518 are acknowledged with thanks. Kwesi Aggrey provided the Knudsen cell mass spectrometric analyses of volatiles in glasses at the University of Hawaii, and Jon Woodhead produced the Pb isotopic and ICP-MS analyses at ANU. Brian Taylor helped with the sampling at sea. We are indebted to Tony Crawford, Keith Crook, R. Wally Johnson, David Hilton, Penny King, Anton le Roex, Colin Macpherson, Alison Shaw, Brian Taylor and Iris van der Zander for various discussions and interest in this study. Reviews by Penny King, Brian Taylor, and especially Richard Arculus greatly improved the manuscript. This research was supported by NSF grants OCE-8511288 and OCE-8723036. This is SOEST Contribution 5986.

REFERENCES

Aggrey, K. W., Muenow, D. W. & Sinton, J. M. (1988). Volatile abundances in submarine glasses from the North Fiji and Lau back-arc basins. *Geochimica et Cosmochimica Acta* **52**, 2501–2506.

Auzende, J.-M., Ishibashi, J.-I., Beaudoin, Y., Charlou, J.-L., Delteil, J., Donval, J.-P., Fouquet, Y., Ildefonse, B., Kimura, H., Nishi, Y., Radford-Knoery, J. & Rellan, E. (2000). Extensive magmatic and hydrothermal activity documented in Manus Basin. *EOS Transactions, American Geophysical Union* **81**, 449, 453.

Bender, J. F., Langmuir, C. H. & Hanson, G. N. (1978). Petrogenesis of basalts from the project FAMOUS area: experimental study from 0 to 15 kbars. *Earth and Planetary Science Letters* **41**, 277–302.

Binns, R. A. & Scott, S. D. (1993). Actively-forming polymetallic deposits associated with felsic volcanic rocks in the eastern Manus backarc basin, Papua New Guinea. *Economic Geology* **88**, 2226–2236.

Byerly, G. R., Melson, W. G. & Vogt, P. R. (1976). Rhyodacites, andesites, ferro-basalts and ocean tholeiites from the Galápagos spreading center. *Earth and Planetary Science Letters* **30**, 215–221.

Chappell, B. W. (1992). Trace element analysis of rocks by x-ray spectrometry. *Advances in X-ray Analysis* **34**, 263–276.

Cooper, P. & Taylor, B. (1987). Seismotectonics of New Guinea: a model for arc reversal following arc–continent collision. *Tectonics* **6**, 53–67.

Cooper, P. & Taylor, B. (1989). Seismicity and focal mechanisms at the New Britain Trench related to deformation of the lithosphere. *Tectonophysics* **164**, 25–40.

Crook, K. A. W., Lisitzin, A. P. & Borissova, I. A. (1997). *Results and Prospects from the Joint USSR Australia USA PNG Geological Study of the Manus Basin during the 21st Cruise of the R/V* Akademik Mstislav Keldysh. *Marine Geology, Special Issue* **142**, 209 pp.

DePaolo, D. J. & Johnson, R. W. (1979). Magma genesis in the New Britain island arc: constraints from Nd and Sr isotopes and trace-element patterns. *Contributions to Mineralogy and Petrology* **70**, 367–379.

Elliott, T., Plank, T., Zindler, A., White, W. & Bourdon, B. (1997). Element transport from slab to volcanic front at the Mariana arc. *Journal of Geophysical Research* **102**, 14991–15019.

Falloon, T. J. & Danyushevsky, L. V. (2000). Melting of refractory mantle at 1·5, 2 and 2·5 GPa under anhydrous and H_2O-undersaturated conditions: implications for the petrogenesis of high-Ca boninites and the influence of subduction components on mantle melting. *Journal of Petrology* **41**, 257–283.

Falloon, T. J., Green, D. H., Hatton, C. J. & Harris, K. L. (1988). Anhydrous partial melting of a fertile and depleted peridotite from 2 to 30 kb and application to basalt petrogenesis. *Journal of Petrology* **29**, 1257–1282.

Falvey, D. A. & Pritchard, T. (1985). Preliminary paleomagnetic result from northern Papua New Guinea: evidence for large microplate rotations. *Transactions of the Circum-Pacific Council for Energy and Mineral Resources* **3**, 593–600.

Fryer, P., Sinton, J. M. & Philpotts, J. A. (1981). Basaltic glasses from the Mariana Trough. In: Hussong, D. M., Uyeda, S. *et al.* (eds) *Initial Reports of the Deep Sea Drilling Project, 60*. Washington, DC: US Government Printing Office, pp. 601–609.

Garcia, M. O., Liu, N. W. K. & Muenow, D. W. (1979). Volatiles in submarine volcanic rocks from the Mariana island arc and trough. *Geochimica et Cosmochimica Acta* **43**, 305–312.

Gill, J.B. (1981). *Orogenic Andesites and Plate Tectonics*. New York: Springer, 390 pp.

Goles, G. G. (1977). Instrumental methods of neutron activation analysis. In: Zussman, J. (ed.) *Physical Methods in Determinative Mineralogy*, 2nd edn. London: Academic Press, pp. 343–370.

Green, D. H. (1971). Composition of basaltic magmas as indicators of conditions of origin: application to oceanic volcanism. *Philosophical Transactions of the Royal Society of London* **268**, 707–725.

Green, D. H. (1973). Contrasting melting relations in a pyrolite upper mantle under mid-oceanic ridge, stable crust and island arc environments. *Tectonophysics* **17**, 285–297.

Green, D. H. & Wallace, M. E. (1988). Mantle metasomatism by ephemeral carbonatitic melts. *Nature* **336**, 459–462.

Hauri, E. K., Shimizu, N., Dieu, J. J. & Hart, S. R. (1993). Evidence for hotspot-related carbonatite melts. *Nature* **336**, 221–227.

Hess, P. C. (1992). Phase equilibria constraints on the origin of ocean floor basalts. In: Phipps Morgan, J., Blackman, D. K. & Sinton, J. M. (eds) *Mantle Flow and Melt Generation at Mid-Ocean Ridges. Geophysical Monograph, American Geophysical Union* **71**, 67–102.

Hey, R. N., Sinton, J. M. & Duennebier, F. K. (1989). Propagating rifts and spreading centers. In: Winterer, E. L., Hussong, D. M. & Decker, R. W. (eds) *The Geology of North America, Vol. N: The Eastern Pacific Ocean and Hawaii*. Boulder, CO: Geological Society of America, pp. 161–176.

Hirose, K. & Kawamoto, T. (1995). Hydrous partial melting of lherzolite at 1 GPa—the effect of H_2O on the genesis of basaltic magmas. *Earth and Planetary Science Letters* **133**, 463–473.

Hirschmann, M. M., Ghiorso, M. S., Wasylenki, L. E., Asimow, P. D. & Stolper, E. M. (1998). Calculation of peridotite partial melting from thermodynamic models of minerals and melts. 1. Review of methods and comparison with experiments. *Journal of Petrology* **39**, 1091–1115.

Hochstaedter, A. G., Gill, J. B., Taylor, B., Ishizuka, O., Yuasa, M. & Morita, S. (2000). Across-arc geochemical trends in the Izu–Bonin arc: constraints on source composition and mantle melting. *Journal of Geophysical Research* **105**, 495–512.

Jaques, A. L. & Green, D. H. (1980). Anhydrous melting of peridotite at 0–15 kb pressure and genesis of tholeiitic basalts. *Contributions to Mineralogy and Petrology* **73**, 287–310.

Johnson, K. T. M. & Sinton, J. M. (1990). Petrology, tectonic setting and the formation of back-arc basin basalts in the North Fiji Basin. *Geologisches Jahrbuch* **92**, 517–545.

Johnson, K. T. M., Dick, H. J. B. & Shimizu, N. (1990). Melting in the oceanic upper mantle: an ion microprobe study of diopsides in abyssal peridotites. *Journal of Geophysical Research* **95**, 2661–2678.

Johnson, R. W. (1976). Potassium variation across the New Britain volcanic arc. *Earth and Planetary Science Letters* **31**, 184–191.

Johnson, R. W. (1977). Distribution and major element chemistry of late Cainozoic volcanoes at the southern margin of the Bismarck Sea, Papua New Guinea. *Report, Australian Bureau of Mineral Resources* **188**.

Johnson, R. W. & Arculus, R. J. (1978). Volcanic rocks of the Witu Islands, Papua New Guinea: the origin of magmas above the deepest part of the New Britain Benioff Zone. *Earth and Planetary Science Letters* **41**, 609–655.

Johnson, R. W., Smith, I. E. M. & Taylor, S. R. (1978). Hot-spot volcanism in St. Andrew Strait, Papua New Guinea: geochemistry of a Quaternary bimodal rock suite. *BMR Journal Australian Geology and Geophysics* **3**, 55–69.

Johnson, R. W., Mutter, J. C. & Arculus, R. J. (1979). Origin of the Willaumez–Manus Rise, Papua New Guinea. *Earth and Planetary Science Letters* **44**, 247–260.

Klein, E. M. & Langmuir, C. H. (1987). Global correlations of ocean ridge basalt chemistry with axial depth and crustal thickness. *Journal of Geophysical Research* **92**, 8089–8115.

Kushiro, I. (1968). The system forsterite–diopside–silica with and without water at high pressures. *American Journal of Science* **267A**, 269–294.

Langmuir, C. H., Klein, E. M. & Plank, T. (1992). Petrological systematics of mid-ocean ridge basalts: constraints on melt generation beneath mid-ocean ridges. In: Phipps Morgan, J., Blackman, D. K. & Sinton, J. M. (eds) *Mantle Flow and Melt Generation at Mid-Ocean Ridges. Geophysical Monograph, American Geophysical Union* **71**, 183–280.

Liu, L. A. S. M. (1989). Geochemistry and petrology of lavas from the Manus Basin Extensional Transform Zone and Manus Spreading Center: implications for source compositions and metasomatic processes in back-arc basins. M.S. thesis, University of Hawaii, 94 pp.

Macpherson, C. G., Hilton, D. R., Sinton, J. M., Poreda, R. J. & Craig, H. (1998). High $^{3}He/^{4}He$ ratios in the Manus backarc basin: implications for mantle mixing and the origin of plumes in the western Pacific Ocean. *Geology* **26**, 1007–1010.

Macpherson, C. G., Hilton, D. R., Mattey, D. P. & Sinton, J. M. (2000). Evidence for an ^{18}O-depleted mantle plume from contrasting $^{18}O/^{16}O$ ratios of back-arc lavas from the Manus Basin and Mariana Trough. *Earth and Planetary Science Letters* **176**, 171–183.

Martinez, F. & Taylor, B. (1996). Backarc spreading, rifting and microplate rotation between transform faults in the Manus Basin. *Marine Geophysical Researches* **18**, 203–224.

Martinez, F. & Taylor, B. (2002). Mantle wedge control on back-arc crustal accretion. *Nature* **416**, 417–420.

McCulloch, M. T. & Gamble, J. A. (1991). Geochemical and geodynamical constraints on subduction zone magmatism. *Earth and Planetary Science Letters* **102**, 358–374.

Nakamura, Y. & Kushiro, I. (1974). Composition of the gas phase in Mg_2SiO_4–SiO_2–H_2O at 15 kbar. *Carnegie Institution of Washington Yearbook* **73**, 255–258.

Nicholls, I. A. & Ringwood, A. E. (1973). Effect of water on olivine stability in tholeiites and the production of silica-saturated magmas in the island-arc environment. *Journal of Geology* **81**, 285–300.

Niu, Y. & Batiza, R. (1991). An empirical method for calculating melt compositions produced beneath mid-ocean ridges. *Journal of Geophysical Research* **96**, 21753–21777.

Niu, Y. & Batiza, R. (1993). Chemical variation trends at fast and slow spreading mid-ocean ridges. *Journal of Geophysical Research* **98**, 7887–7902.

Niu, Y., Waggoner, D. G., Sinton, J. M. & Mahoney, J. J. (1996). Mantle source heterogeneity and melting processes beneath seafloor spreading centers: the East Pacific Rise, 18°–19°S. *Journal of Geophysical Research* **101**, 27711–27733.

Norrish, K. & Hutton, J. T. (1977). An accurate x-ray spectrographic method for the analysis of a wide range of geological samples. *Geochimica et Cosmochimica Acta* **33**, 431–441.

Plank, T. & Langmuir, C. H. (1988). An evaluation of the global variations in the major element chemistry of arc basalts. *Earth and Planetary Science Letters* **90**, 349–370.

Plank, T. & Langmuir, C. H. (1992). Effects of the melting regime on the composition of the oceanic crust. *Journal of Geophysical Research* **97**, 19749–19770.

Price, R. C., Johnson, L. E. & Crawford, A. J. (1990). Basalts of the North Fiji Basin: the generation of back arc basin magmas by mixing of depleted and enriched mantle sources. *Contributions to Mineralogy and Petrology* **105**, 106–121.

Saunders, A. D. & Tarney, J. (1979). The geochemistry of basalts from a back-arc spreading centre in the East Scotia Sea. *Geochimica et Cosmochimica Acta* **43**, 555–572.

Schneider, M. E. & Eggler, D. H. (1986). Fluids in equilibrium with peridotite minerals: Implications for mantle metasomatism, *Geochimica Cosmochimica Acta*, **50**, 711–724.

Sekine, T. & Wyllie, P. J. (1982). The system granite–peridotite–H_2O at 30 kbar, with applications to hybridization in subduction zone magmatism. *Contributions to Mineralogy and Petrology* **81**, 190–202.

Shaw, A. M., Hilton, D. R., Macpherson, C. G. & Sinton, J. M. (2001). Nucleogenic neon in high $^{3}He/^{4}He$ lavas from the Manus back-arc basin: a new perspective on He–Ne decoupling. *Earth and Planetary Science Letters* **194**, 53–66.

Shaw, D. M. (1970). Trace element fractionation during anatexis. *Geochimica et Cosmochimica Acta* **34**, 237–243.

Sinton, J. M. (1997). The Manus Spreading Center near 3°22′S and the Worm Garden hydrothermal site: results of Mir2 submersible dive 15. *Marine Geology* **142**, 207–209.

Sinton, J. M. & Fryer, P. (1987). Mariana Trough lavas from 18°N: implications for the origin of back arc basin basalts. *Journal of Geophysical Research* **92**, 12782–12802.

Sinton, J. M., Wilson, D. S., Christie, D. M., Hey, R. N. & Delaney, J. R. (1983). Petrological consequences of rift propagation on oceanic spreading ridges. *Earth and Planetary Science Letters* **62**, 193–207.

Sinton, J. M., Smaglik, S. M., Mahoney, J. J. & Macdonald, K. C. (1991). Magmatic processes at superfast spreading mid-ocean ridges: glass compositional variations along the East Pacific Rise, 13°–23°S. *Journal of Geophysical Research* **96**, 6133–6155.

Stolper, E. & Newman, S. (1994). The role of water in the petrogenesis of Mariana trough magmas. *Earth and Planetary Science Letters* **121**, 293–325.

Sudo, A. & Tatsumi, Y. (1990). Phlogopite and K-amphibole in the upper mantle: implication for magma genesis in subduction zones. *Geophysical Research Letters* **17**, 29–32.

Sun, S. S. & McDonough, W. F. (1989). Chemical and isotopic systematics of ocean island basalts: implications for mantle composition and processes. In: Saunders, A. D. & Norry, M. J. (eds)

Magmatism in the Ocean Basins. Geological Society, London, Special Publications **42**, 313–345.

Sweeney, R. J. (1994). Carbonatite melt compositions in the Earth's mantle. *Earth and Planetary Science Letters* **128**, 259–270.

Tarney, J., Saunders, A. D. & Weaver, S. D. (1977). Geochemistry of volcanic rocks from the island arcs and marginal basins of the Scotia Sea region. In: Talwani, M. & Pitman, W. (eds) *Island Arcs, Deep Sea Trenches, and Back-Arc Basins. Maurice Ewing Series, American Geophysical Union* **1**, 367–377.

Tatsumi, Y. (1989). Migration of fluid phases and genesis of basalt magmas in subduction zones. *Journal of Geophysical Research* **94**, 4697–4707.

Tatsumi, Y. & Kogiso, T. (1997). Trace element transport during dehydration processes in the subducted oceanic crust: 2. Origin of chemical and physical characteristics in arc magmatism. *Earth and Planetary Science Letters* **148**, 207–221.

Tatsumi, Y., Hamilton, D. L. & Nesbit, R. W. (1986). Chemical characteristics of fluid phase released from a subducted lithosphere and the origin of arc magmas: evidence from high-pressure experiments and natural rocks. *Journal of Volcanology and Geothermal Research* **29**, 293–309.

Taylor, B. (1979). Bismarck Sea: evolution of a back-arc basin. *Geology* **7**, 171–174.

Taylor, B. & Karner, G. (1983). On the evolution of marginal basins. *Reviews of Geophysics and Space Physics* **21**, 1727–1741.

Taylor, B., Crook, K. A. W., Sinton, J. M. & Peterson, L. (1991). Manus Basin, Papua New Guinea, SeaMARC II sidescan imagery and bathymetry, scale 1:250,000. In: *Pacific Seafloor Atlas, Sheets 1–6*. Honolulu: Hawaii Institute of Geophysics.

Taylor, B., Crook, K. A. W. & Sinton, J. M. (1994). Extensional transform zones and oblique spreading centers. *Journal of Geophysical Research* **99**, 19707–19718.

Tufar, W. (1989). Modern hydrothermal activity, formation of complex massive sulfide deposits and associated vent communities in the Manus back-arc basin (Bismarck Sea, Papua New Guinea). *Mitteilungen der Österreichischen Geologischen Gesellschaft* **82**, 183–210.

Wallace, M. E. & Green, D. H. (1988). An experimental determination of primary carbonatite magma composition. *Nature* **335**, 343–346.

Woodhead, J., Eggins, S. & Gamble, J. (1993). High field strength and transition element systematics in island arc and backarc basalts: evidence for multi-phase melt extraction and a depleted mantle wedge. *Earth and Planetary Science Letters* **114**, 491–504.

Woodhead, J. D. & Johnson, R. W. (1993). Isotopic and trace-element profiles across the New Britain island arc, Papua New Guinea. *Contributions to Mineralogy and Petrology* **113**, 479–491.

Woodhead, J. D., Eggins, S. M. & Johnson, R. W. (1998). Magma genesis in the New Britain island arc: further insights into melting and mass transfer processes. *Journal of Petrology* **39**, 1641–1668.

Wyllie, P. J. & Sekine, T. (1982). The formation of mantle phlogopite in subduction zone hybridization. *Contributions to Mineralogy and Petrology* **79**, 375–380.

Yaxley, G. M., Crawford, A. J. & Green, D. H. (1991). Evidence for carbonatitic metasomatism in spinel peridotite xenoliths from western Victoria, Australia. *Earth and Planetary Science Letters* **107**, 305–317.

Yoder, H. S., Jr & Tilley, C. E. (1962). Origin of basalt magmas: an experimental study of natural and synthetic rock systems. *Journal of Petrology* **3**, 342–532.

You, C.-F., Castillo, P. R., Gieskes, J. M., Chan, L. H. & Spivak, A. J. (1996). Trace element behavior in hydrothermal experiments: implications for fluid processes at shallow depths in subduction zones. *Earth and Planetary Science Letters* **140**, 41–52.